We are IntechOpen, the world's leading publisher of Open Access books Built by scientists, for scientists

5,000
Open access books available

125,000
International authors and editors

140M
Downloads

Our authors are among the

154
Countries delivered to

TOP 1%
most cited scientists

12.2%
Contributors from top 500 universities

WEB OF SCIENCE™

Selection of our books indexed in the Book Citation Index in Web of Science™ Core Collection (BKCI)

Interested in publishing with us?
Contact book.department@intechopen.com

Numbers displayed above are based on latest data collected.
For more information visit www.intechopen.com

Chapter

Fluorescence Fluctuation Techniques for the Investigation of Structure-Function Relationships of G-Protein-Coupled Receptors

Robert T. Youker and Danielle Voet

Abstract

G-protein-coupled receptors (GPCRs) are seven transmembrane receptors that form the largest superfamily of signaling proteins, and the family members function in a diverse array of metabolic pathways including cardiac function, immune response, neurotransmission, smell, taste, cell differentiation and growth, and vision. It is becoming clear that alteration in the quaternary structure of the GPCR receptor can have a profound impact on signaling capabilities. Biochemical, biophysical, physiological, x-ray crystallographic, and computational methods have been used over the last 40–50 years to study the structure and function of GPCRs. Evidence from these studies confirm that GPCRs can be organized as monomers, dimers, and higher-order oligomers. However, many times, these methods require extraction of the receptor from its native environment and high levels of expression and only provide a snapshot of information. A need arose for techniques that could measure the assembly and disassembly of receptors at few-to-single molecule resolution in their native environment at fast time scales. In the last 20 years, fluorescence fluctuation techniques have filled this need and provided new insight into the dynamics of GPCR organization in the absence and presence of ligands, agonists, and antagonists. In this book chapter, we provide a brief introduction to GPCR structure and function [Section 1]. An overview of the theoretical basis for fluorescence fluctuations techniques (FFTs) and how FFTs can be used to study the oligomeric structure of GPCRs in live and fixed cells is explained [Section 2]. We discuss the advantages and limitations of FFTs [Section 3], and finally, we summarize select case studies on GPCR structure and function revealed by FFT experiments [Section 4].

Keywords: fluorescence spectroscopies, molecular brightness, GPCR, oligomer, dimer, SpIDA, protein dynamics

1. Introduction

G-protein-coupled receptors (GPCRs), also known as hepta-helical or seven transmembrane receptors, form the largest superfamily of signaling proteins that comprise 3–5% of genes in animals with approximately 1000 and 800 genes in the human and mice genomes, respectively [1–4]. GPCRs are evolutionarily conserved

from single cell excavates – asymmetric protists that usually contain an "excavated" feeding groove – to multicellular animals. Recent phylogenetic analysis of 75 genomes suggest evolution of these ancient GPCRs and associated cytoplasmic signaling machineries occurred through lineage-specific diversification with repeated domain shuffling (**Figure 1**) [5]. Many of the gene families needed for GPCR signaling were present in the last common ancestor of eukaryotes [6–9]. Interestingly, architectural diversification of the N-terminal protein domain of GPCRs was concomitant with the diversification of these ancient protein families [10]. These observations support the theory that the GPCR core signaling machinery evolved first followed by extensive receptor radiation and selective pressures (positive and negative) may have affected evolution of GPCR subgroups differently [5, 11].

The extensive diversification of GPCRs was most likely necessary as eukaryotes evolved from unicellular to multicellular organisms and to exploit new environmental niches, thus sensing and responding to novel stimuli [12]. GPCR family members can be activated by an extraordinary array of molecules that include amines, amino acids, cytokines, glycoproteins, hormones, ions, nucleotides, peptides, and even photons of light, in the case of the Rhodopsin family. Multiple classification systems have been developed for GPCRs (e.g. A-F system and GRAFS system) using a variety of approaches that include motif-based, pharmacological-based, machine learning, or phylogenetic tools [3, 13–15]. The GRAFS system relies on structural and phylogenetic information to classify Metazoan GPCRs [2, 3, 10]. The GRAFS system divides GPCRs into the Glutamate (Class C of A-F system), Rhodopsin (Class A), Adhesion (Class B), Frizzled (Class F), and Secretin (Class B) families. This classification system has been extended to several lineage-specific GPCR families (insect odorant receptors, nematode chemoreceptors, vertebrate vomeronasal receptors) and non-metazoan members such as cAMP (Class E), GPR-108-like families and ITR-like families [16]. The Fungi Ste2 (Class D), Ste3 (Class D), and Git3 receptors and the plant abscisic receptor are also categorized as GPCRs [17, 18]. An important difference between the two widely used classification systems are that GRAFS further divides class B into the Secretin and Adhesion receptor subfamilies, while the A-F system does not.

A majority of physiological functions, including cell differentiation and growth, immune response, metabolism, neurotransmission, smell, taste, and vision are regulated by GPCR signaling. Not surprisingly, disruption of GPCR signaling can cause a wide variety of disease such as cardiac dysfunction, diabetes, nervous system disorders, obesity, inflammation, and even cancer. Estimates range from 30 to 40% of all FDA approved drugs target GPCRs given the central roles of these receptors in human physiology [19, 20]. There are greater than 300 protein structures representing 64 unique GPCRs and the vast majority of solved structures belong to the class A subfamily (GPCR database, accessed May 7, 2020, [21]). Structurally, GPCRs all contain an extracellular domain, a counter-clockwise transmembrane helical bundle, and an intracellular domain. The extracellular domains have the least degree of conservation and vary in size and shape. For example, most class A members have small extracellular domains compared to class B (secretion family) and class C (glutamate family) members that possess long N-terminal domains of approximately 120 and 600 amino acids, respectively (**Figure 1**).

Most GPCRs bind ligands directly to the extracellular N-terminus and/or a binding pocket composed of the extracellular region and transmembrane helices. Typically, GPCRs signal through a heterotrimeric G-protein complex whereby ligand binding to the receptor causes a conformational change and the receptor acts as a guanine nucleotide exchange factor (GEF) to activate the alpha-subunit (Gα) by facilitating GTP binding [22]. Activated Gα dissociates from the Gβγ subunits to allow interaction with downstream effectors such adenylate cyclase,

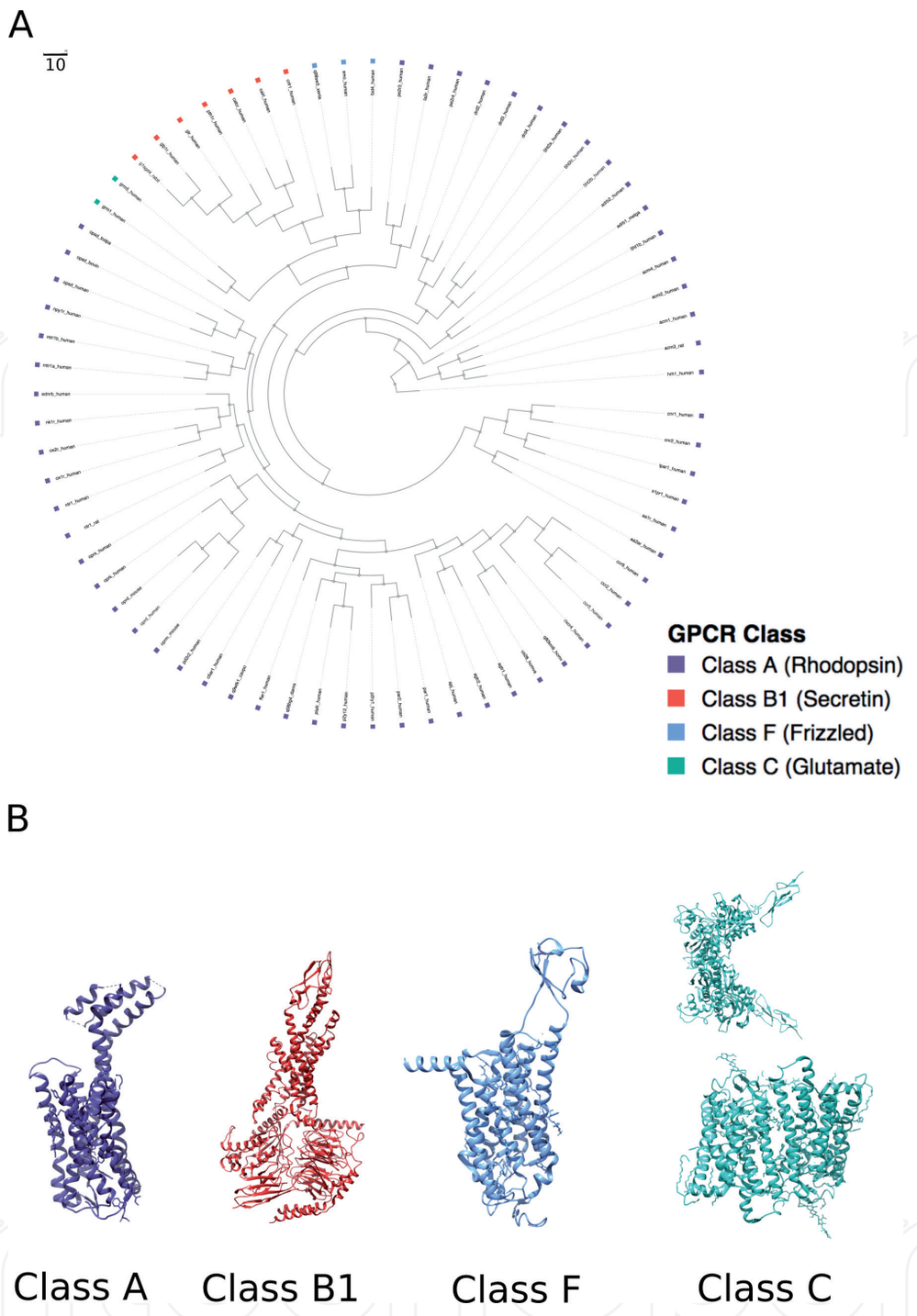

Figure 1.
Neighbor-joining phylogenetic tree of select human GPCRs and representative crystal structures. (A) Information for GPCR phylogenetic tree (steps used): Seventy human GPCRs with crystal structures deposited in GPCRdb were used to construct neighbor-joining distance calculation on conserved segments of sequence/structure with bootstrapping (10 replicates) with regular branch lengths depicted. GPCR classes A (purple), B1 (red), F (light blue), and C (green) are represented. Scale bar = 10. Tree constructed using PHYLIP and jsPhyloSVG packages implemented through GPCRdb website. (B) Crystal structures of class A (serotonin receptor, PBD: 6bqh), class B1 (glucagon receptor, PDB: 6lmk), class F (frizzled 4 receptor, PDB: 6bd4), and class C (extracellular domain from metabotropic glutamate receptor 3 (PDB: 2e4w) and 7TM from bovine rhodopsin (PDB: 1gzm) as a structural model to represent class because no full-length structures exist, https://doi.org/10.1038/aps.2011.186). Structures are colored to match key in part a.

or phospholipase C (PLC), leading to a second messenger signaling cascade [22]. The Gβγ dimeric complex recruits G-protein-coupled receptor kinase (GRK) to the activated receptor and the GRK phosphorylates the GPCR on serine or threonine residues residing in the intracellular C-terminal tail, or the third intracellular loop [23–25]. Phosphorylation of the receptor leads to β-arrestin binding followed by

adaptor and clathrin recruitment that triggers endocytosis of the receptor to attenuate signaling. Concomitantly, the Gα subunit and regulators of G-protein signaling (RGS) facilitate re-association of the heterotrimeric complex through GTP hydrolysis, thus resetting the switch for another round of signaling. The GPCR is then either recycled back to the cell surface or degraded in the lysosome and this completes the receptor life cycle (for review see [22]). Recent evidence suggests that in some cases, GPCRs can signal from early endosomes, trans-Golgi network (TGN), mitochondria, and nuclear membranes (for review see [1, 26, 27]). This observed intracellular GPCR signaling is dynamic and is thought to play an important role in synaptic plasticity, learning and memory [26].

In addition, G-protein independent signaling through arrestins, arrestin domain containing proteins (ARDCs) and GRKs has been reported (for review see [4, 28–30]). For example, arrestins can bind to mitogen-activated protein kinase (MAPK) pathway members both at the plasma membrane and from endosomal membranes to trigger G-protein independent MAPK signaling [31, 32]. Interestingly, arrestin activation of extracellular-signal-regulated kinase (ERK) appears to bias cytoplasmic instead of nuclear MAPK signaling possibly through inhibition of ERK translocation to the nucleus [32].

The ability of GPCRs to activate G-protein-mediated, arrestin-mediated, or another potential signaling pathway is called biased signaling [33]. This signaling complexity is due to the ability of GPCRs to bind to multiple ligands, interact with an array of regulators (as mentioned above) and cross-regulate each other leading to a balanced cellular/functional response [34, 35]. The signaling complexity of GPCRs is also due to the dynamic quaternary state of the receptors. The quaternary state of a protein describes whether it is composed of one, or more, folded chains of amino acids. GPCRs are well known to function as monomers and dimers but can also form larger quaternary structures, termed higher-order oligomers that contain three, or more, molecules in a complex [36]. The quaternary state of the receptor can affect its ability to be activated and may influence the type of downstream signaling pathway that is engaged, such as plasma membrane versus intracellular membrane signaling. Therefore, it is vitally important to quantify temporal and spatial GPCR conformational changes in order to gain insight into GPCR signaling [37].

There are a plethora of experimental methods to measure GPCR oligomeric structure that can be classified as biochemical, biophysical, physiological, x-ray crystallographic, and computational [38]. Biochemical methods include co-immunoprecipitation (co-IP) and blue native PAGE (BN-PAGE) that require extraction of the protein from their native cellular membranes. Förster resonance energy transfer (FRET), fluorescence complementation, and fluorescence recovery after photobleaching (FRAP) are examples of biophysical methods where receptors are labeled and measured in their native environment [37, 39]. Total internal reflection fluorescence microscopy (TIRFM), single-molecule imaging, and spatial intensity distribution analysis (SpIDA) are considered physiological methods for studying GPCRs in live and fixed cells. Methods such as x-ray crystallography, NMR spectroscopy and cryo-electron microscopy (cryo-EM) are capable of determining structures at atomic resolution, and only NMR can determine three-dimensional protein structures in solution [40]. Finally, computational methods, such as molecular dynamic (MD) simulations, provide insight into dynamic behavior of GPCRs at the atomic level based on x-ray crystallographic structures. In the last two decades, fluorescence fluctuation techniques have become a vital tool for measuring the dynamic oligomeric changes of proteins, including GPCRs, because of their single molecule sensitivity, high spatial resolution, and ability to measure physiologically-relevant concentrations in live cells [41–43]. We will focus on these existing and newly

developed fluorescence techniques and no other well established and traditionally used biophysical/biochemical techniques to study GPCRs that are mentioned above (for reviews see [37–40]).

In this book chapter, we provide an overview of the theoretical basis for fluorescence fluctuations techniques (FFTs) and how FFTs can be used to study the oligomeric structure of GPCRs in live and fixed cells [Section 2]. We discuss the advantages and limitations of FFTs [Section 3]. Finally, we summarize select case studies on GPCR structure and function revealed by FFT experiments [Section 4].

2. Overview of fluorescence fluctuation techniques (FFTs)

Fluorescence fluctuation spectroscopy (FFS) techniques, a.k.a. FFTs, refers to a suite of spectroscopic/microscopic techniques that exploit the fluctuations detected in the signal emitted from a fluorescent molecule to extract molecular dynamic information, such as diffusion rate and oligomeric size of the molecule. Measurements can be made on purified molecules *in vitro* in a cuvette, or on molecules inside live cells with the aid of a confocal microscope. FFTs can be classified based on method of collection of the fluorescence fluctuation information, such as a spot method versus scanning method, or by how the information is analyzed, such as space, time, or both (**Figure 2**). The following sections describe several of the most common FFTs that have been developed, especially for GPCR studies, but are not an exhaustive list of all developed applications (for in-depth review see [41, 44–46]).

2.1 Fluorescence correlation spectroscopy (FCS)

Fluorescence correlation spectroscopy (FCS) was developed in the 1970s at the Karolinska Institute in Stockholm and Cornell University in the U.S. [47, 48]. Today, it is a common spot method implementation, whereby the signal fluctuations from a small volume (>1 femtoliter) are observed, recorded, and an autocorrelation function (ACF) is calculated to determine molecular processes. The main process causing the fluctuations are the diffusion of the fluorescent molecules through the detection volume, but other processes that create fluctuations can be measured, including active transport, flow, rotational diffusion, excited state transitions, chemical reactions, and bleaching [49, 50]. FCS was used in the seminal experiments by Magde, Elson, and Webb to measure diffusion of DNA and kinetics of ethidium bromide binding [47]. FCS measurements were confined to *in vitro* (cuvette) setups because cell experiments using widefield microscopes had "large" excitation and detection volumes that prevented observation of fluorescence fluctuations. Invention of confocal and two-photon excitation microscopies, with greatly reduced volumes, expanded the technique to living systems in the 1990s.

The primary parameters determined from FCS measurements are the average diffusion rate and concentration of observed molecules (**Table 1**). A variation of FCS called fluorescence cross-correlation spectroscopy (FCCS) requires labeling of two molecules with different fluorescent dyes and can be used to study molecular interactions [41]. The amplitude of the ACF plot is inversely proportional to the average number (N) of fluorescent molecules traversing the detection volume and gives FCS a large dynamic range with the ability to measure pico- to nanomolar concentrations of molecules with background fluorescence and detector technology limiting cellular measurements to ~1–400 nM [45, 51]. Concentrations higher than a couple hundred nanomolars cause a reduction in fluctuations and inability to calculate the ACF. Diffusion of fluorescent molecules can be measured over six

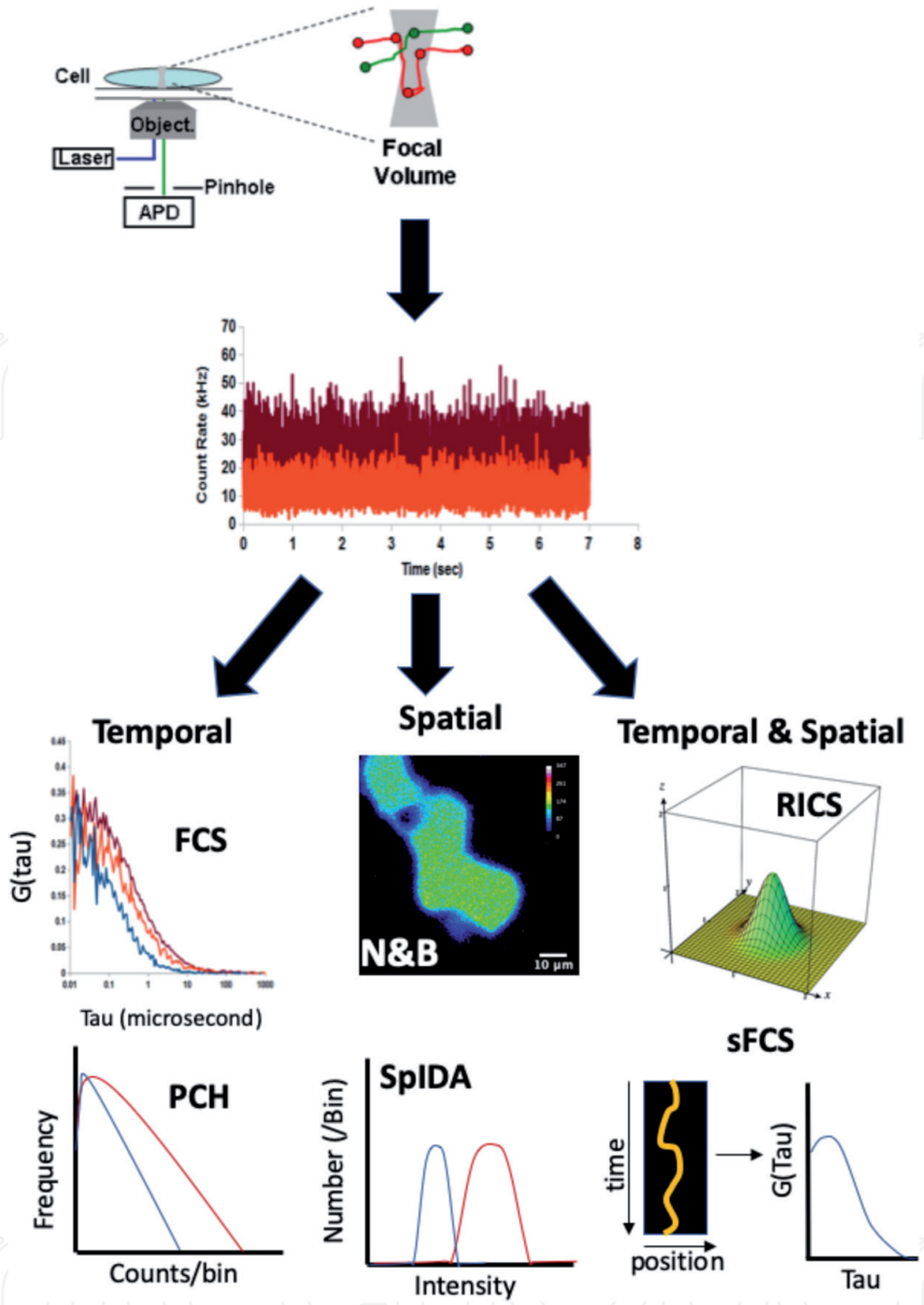

Figure 2.
Categories of fluorescence fluctuation spectroscopies (FFS). Fluorescence signal is recorded from molecules moving through focal volume (~1 femtoliter) of a confocal or two-photon microscope. The fluctuations in the signal can be analyzed to extract molecular parameters (e.g. diffusion and brightness) in the temporal, spatial, or temporal and spatial domains. Representative techniques that analyze in the temporal domain are FCS and PCH. Techniques that analyze in the spatial domain include N&B and SpIDA. The RICS and sFCS analyses exploit information in the temporal and spatial domains. For FCS, blue curve represents fast diffusing species, and dark red curve represents slower species. For PCH and SpIDA, the blue curves represent small species (e.g. monomers) and the dark red curves represent larger species (e.g. oligomers).

orders of magnitude using FCS (microsecond to millisecond) with the limitations at the upper limit being photobleaching for slowly moving particles/complexes and inability to detect fluctuations, as mentioned above. FCS has been used to measure the diffusion and size of nucleic acids, lipids, individual proteins, and protein complexes in live cells. Recent examples of processes investigated with FCS/FCCS include viral capsid assembly, mRNA diffusion, enzyme subunit dissociation, system wide measurements of protein diffusion in yeast, gene expression

Technique name	Temporal resolution	Spatial resolution	Parameters extracted
FCS/FCCS	Nanosecond to microsecond	–[b]	Mobility, concentration, interaction
PCH/moment	–[a]	–[b]	Brightness, oligomerization
sFCS/sFCCS	Microsecond to millisecond	Diffraction limited	Mobility, concentration, interaction
RICS/cc-RICS	Microsecond to millisecond	0.8 μm	Mobility, concentration, interaction maps
ICS/ICCS	—	0.5 μm	Concentration, oligomerization
N&B/cc-N&B	—	Diffraction limited	Mobility, concentration, interaction maps
SpIDA	—	<30 nm[c]	Concentration, oligomerization
FIF	—	–[d]	Abundance and stability of oligomers

[a]*Depends on binning and detector characteristics.*
[b]*Spot measurement.*
[c]*Assuming sufficient signal-to-noise ratio (SNR).*
[d]*Depends on size and shape of ROIs and SNR.*

Table 1.
Comparison of select fluorescence fluctuation spectroscopies.

profiles, protein-lipid interactions, and receptor-ligand interactions [52–60]. FCCS can be used to quantify and distinguish different populations of receptors, protein complexes, protein-lipid interactions, and protein-DNA interactions [61–69]. FCS/FCCS are spot measurements where the excitation laser is kept immobile leading to high temporal resolution but measurements in several locations are required if a larger area of the specimen is to be analyzed.

Importantly, for multicomponent systems — where there are two different dye labeled molecules or different states of the same species — the diffusion rates for the species must differ by ~1.6-fold or greater in order for FCS to resolve the multiple species [70]. For this reason and others listed below (see Section 2.2), a large body of additional FFTs have been developed based on photophysical properties of molecules. Techniques such as photon counting histogram (PCH) analysis and fluorescence intensity distribution analysis (FIDA) exploit moments of the fluorescent signal (i.e. mean, variance, higher order) to determine molecular brightness (ε) and resolve multicomponent systems [71–74]. Methods centered around moment analysis and related FFTs are discussed in Section 2.2 to below.

2.2 Photon counting histogram (PCH) and higher-order analyses

2.2.1 PCH and FIDA analyses

Intensity (1st moment) and variance (2nd moment) information collected during FCS experiments can be used to determine protein size and *N* provided the concentrations of investigated molecules are constant or homogenous during measurement (e.g. amount of receptor monomer and dimer). Importantly, biological systems are complex and the fluorescently labeled molecules/structures usually exist in multiple states whose concentrations are changing temporally. Furthermore, the molecule's brightness contributes nonlinearly to the ACF and, therefore, molecular concentrations cannot be unambiguously determined without

knowing the molecular brightness (ε) [70, 75]. Thus, it can be difficult to extract protein size and *N* accurately using FCS with complex systems [70, 75].

Both PCH and fluorescent intensity distribution (FIDA) analyses do not suffer from the same limitations as FCS. These analyses measure the ε and associated fluorescence intensity distributions to resolve species in multicomponent systems and are amenable to systems where the species have similar diffusion rates [71–74]. The two techniques are considered "mathematically equivalent" and only differ in their treatment of the microscope point spread function (for explanation see, [76]). To implement these techniques, photon counts per sampling time are plotted versus frequency and then fitted using theoretical models to determine *N* and ε, expressed as counts per second per molecule, of the different species. Importantly, the same fluorescent traces used to calculate ACF for FCS analysis can also be used to calculate histograms for PCH analysis. In fact, several commercial hardware/software implementations provide FCS and PCH analysis simultaneously during data acquisition (e.g. Zeiss, Picoquant). Both PCH and FIDA techniques are routinely used to measure protein oligomerization in cells and cellular organelles [67, 77–80]. Homodimers were detected for serotonin 5-hydroxytryptamine 2C (5-HT2C) receptor using FCS and PCH analyses [81–83]. In one study, PCH analysis of freely diffusing class A GPCRs (5-HT2A, α1b-AR, β2-AR, M1, M2, and D1) were observed to be predominantly homodimers in the plasma membrane of HEK293 cells [82]. The stoichiometric binding of ligands to several GPCRs (chemokine, peptide, and small-molecule ligands) was detected using FIDA in a high-throughput assay and similar results were obtained compared to traditional radioligand binding experiments [84].

A mathematically equivalent approach to PCH/FIDA is moment analysis, based on Mandel's Q-parameter, and provides the same information [85–87]. Moment analysis can be difficult in small cells, such as bacteria, because the cell volume can be easily bleached and the cell only partially overlaps with the microscope point spread function (PSF) that can negatively influence intensity fluctuations. These two problems can cause error in brightness calculations [88, 89]. A modified Q-parameter measurement called mean Q-value of segmented photon count data (MSQ) combined with axial scans was developed to overcome these unique challenges faced in cells that are small [89].

2.2.2 Fluorescence cumulant analysis (FCA)

An approach similar to PCH is fluorescence cumulant analysis (FCA). This method employs cumulant functions in place of probability distribution functions and the same photon-counting data used for PCH can be analyzed by FCA [90]. Muller found that FCA gave identical ε and *N* values as PCH and both methods are limited to data sampling times shorter than the diffusion times of the molecules. In contrast to PCH, the FCA theory can be expanded through analytical expressions (e.g. 2nd factorial cumulant) to overcome this limitation and be extended to arbitrary sampling times [90]. FCA is also suited for data containing random independent events because of the additive properties of cumulants that simplify the analysis.

2.2.3 Temporal extension of PCH, FIDA, and FCA

PCH, FIDA, and FCA provide a snapshot of *N* and ε of molecules but not dynamic, or temporal information. These techniques can be modified to extract temporal information through recording multiple counting intervals simultaneously. These time-binned versions of PCH, FIDA, and FCA are called photon

counting multiple histogram (PCMH), fluorescence intensity multiple distribution analysis (FIMDA), and time-integrated fluorescence cumulant analysis (TIFCA), respectively [91–95]. These techniques apply a global analysis, consideration of many dwell-times, to a set of photon count histograms, thus improving signal-to-noise (S/N) ratio of the data and allowing resolution of fluorescent species by both time-dependent (e.g. translational diffusion) and time-independent (e.g. N and ε) parameters.

Recently, a modified version of PCH was developed called correlated PCH (cPCH) that is a generalization of dual-color PCH analysis and combines aspects of FCS, PCH and moment analysis [96, 97]. This inherently dual-channel technique can also be applied to single channel measurements and histograms from the same channel, or different channels are acquired and analyzed from different timepoints. The application of cPCH involves calculating photon counting histograms where the time bins occur at time-differences (τ) between the two detection channels. This allows the analysis of correlation and amplitude of the signal simultaneously. The cPCH method is described to be less computationally intensive and to provide a better approximation for the diffusion dependence of the molecular species compared to PCMH, FIDA, and TIFCA. As proof of concept, Scales and Swain present simulated data for ligand binding to a receptor that has two-binding sites [96]. Scales and Swain lay the theoretical foundation for cPCH but only provide simulations to provide proof of concept and it remains to be seen if the full potential of this technique is realized using real experimental data. In fluorescence intensity and lifetime distribution analysis, lifetime data of the fluorescent species can also be included to provide an additional parameter to resolve the investigated molecules [98]. Photon arrival time distributions can also be used to measure ε and correlation functions simultaneously for measuring macromolecular interactions through the analysis of two-dimensional photon pair histograms [99].

The development of these moment/cumulant techniques extended the sensitivity and resolution capabilities of measuring complex mixtures of fluorescent macromolecules compared to FCS/FCCS. The subsequent extension of these techniques to a global analysis that incorporates temporal information allowed measurement of molecular dynamics. Dual-color versions of these techniques allow the observation of two different labeled fluorescent macromolecules [73, 97]. However, these spot techniques — at the time — were cumbersome for measurements involving multiple, or large region of interests (ROIs). This necessitated the development of scanning FFTs and multiplexing approaches to acquire spatial information across large regions of samples, such as entire cells or tissues (Section 2.3).

2.3 Scanning FFTs (single and multiplexing)

2.3.1 Scanning and multiplexing FCS

In the 1990s, Koppel et al. linearly scanned the laser across samples to measure, with high spatial resolution, the concentration dynamics of fluorescently-labeled DNA [100]. This technique is called scanning mode FCS (sFCS) and allows the measurement of a larger area of the specimen without the hassle of multiple time-consuming single point measurements (for review see [46]). In sFCS, fluctuations are collected in adjacent volumes, at a fast rate, and in the same volume during different orbits, at a slower rate, thus spatial and temporal information are encoded in the data. This allows for correction of slow sample movements that can interfere with analysis in spot measurements like FCS. The increased spatial resolution achieved with sFCS is at the expense of decreased temporal resolution but for most measurements in live cells this is not a major

issue because molecules are diffusing at rates of 0.1 μm^2/sec (membrane proteins) to 25 μm^2/sec (soluble proteins) that is within the temporal resolution of sFCS (microsecond to millisecond) (**Table 1**). The sFCS approach provides better signal-to-noise ratio, greatly reduced chance of photobleaching, and better accuracy for measuring macromolecules with slow dynamics. Initial implementations of sFCS kept the laser stationary and moved the sample but recent setups move the laser beam instead and linear and raster-scanned patterns can be used, leading to different spatial and temporal resolutions [46].

One motivation for multiplexing FCS measurements was due to the need to have single molecule sensitivity and high-spatial resolution to measure a large number of samples in biochip microarray analysis, both during fabrication and implementation of the chip.

Multiplexing of a spot method such as FCS requires the acquisition of fluorescence fluctuations from multiple ROIs in parallel without sacrificing temporal resolution (micro-to-nanoscale). Many strategies have been used to multiplex FCS for confocal microscopes and most techniques employ an array of detectors and custom optical elements to create multifocal excitation spots and detection [101–103].

Strategies used to create multifocal spots include, the use of a 2 × 2 fan-out diffractive optical element, parallel fiber optics, and spatial light modulators [101, 103–105]. These early attempts at multiplexing relied on single photon avalanche photodiodes (SPAD) and photomultiplier tubes (PMTs) due to their high sensitivity and response times (for review of detectors see [43]). However, only small numbers of excitation volumes (4–7) could be generated ranging from PMT, SPAD, and complementary metal oxide semiconductor (CMOS) detectors [101, 103, 105]. Many groups directed their efforts toward implementing electron multiplying charged coupled devices (EMCCDs) because the detectors have high quantum efficiencies, single molecule sensitives, and the flexible detection area with microsecond resolution [106]. A custom fabricated CMOS single photon detector has been shown to collect 64 channels, an 8-fold improvement on earlier studies [107]. A multiplexed setup measuring five ROIs measured the dynamics of the heat shock transcription factor in the nucleus of heat stressed mammalian cells [108]. Confocal volumes need to be sparsely separated (10 or more pixels) in order to avoid cross-talk between signals, limiting confocal multiplexing approaches. One way to circumvent this limitation is to use a spinning disk confocal microscope that can scan a large number (1000s) of widely spaced pinholes temporally across the sample [109]. In this approach, each pixel is only excited for a brief period of time, leading to reduced signal-to-noise ratios.

Both confocal and spinning disk multiplexing approaches suffer from issues with interference from out-of-focus light restricting these techniques to thin samples. Employing total internal reflection (TIR) microscopy, or single-plane illumination microscopy (SPIM) can eliminate this problem and extend multiplexed FCS to thick biological samples [44]. Most SPIM-FCS microscopy have a larger volume compared to confocal because two medium-NA (0.8) objectives are needed to create the plane for illumination and detection [102, 110, 111]. This type of FCS imaging has been used to record ~1 million ACFs simultaneously at 25 frames per second using next generation scientific CMOS detectors [102]. These custom-built systems have mostly been used for detecting dyes and fluorescent beads in solution for proof-of-concept and only a handful of studies performed in cells and organisms have been reported to date [110]. SPIM-FCS and TIR-FCS have reduced bleaching and photodamage compared to other multiplexed FCS approaches because of the 100 nm illumination plane for TIR and ~ 1.0-μm light beam width for SPIM-FCS. Recently, SPIM-FCS has also been extended to a two-color version to investigate molecular interactions [112]. Combining single spot FCS measurements with

automation to create a high-throughput workflow is an alternative to multiplexing and can be easier to implement with biological specimens [113, 114].

2.3.2 Raster image correlation spectroscopy (RICS)

Raster image correlation spectroscopy (RICS) is an imaging analog of FCS that extracts an averaged (2D) spatial ACF from a series of images acquired by a laser scanning confocal microscope [115–117]. The inherent time information encoded in the scanned image(s) can be used to measure molecular dynamics at microsecond, millisecond, and second timescales depending on if the correlation is calculated from pixels that are adjacent, in successive lines, or successive frames, respectively. The ACFs for immobile species have an isotropic Gaussian function, while species with diffusive behavior have a stretched Gaussian in the direction of the fast scanning. Therefore, the ACF in RICS is a product of the correlations due to diffusion and scanning. This aspect of the analysis makes RICS better suited for measuring anisotropic behavior (diffusion rate varying in space and time) compared to traditional single spot FCS. Processes such as auxin transporter diffusion in plant cell plasma membrane, dynamics of adhesion complex protein paxillin, thyrotropin-releasing hormone receptor diffusion under cholesterol depletion, and Ras nanoclustering in plasma membrane have been studied using RICS [117, 117–120]. RICS was combined with 3D-orbital tracking and general polarization analysis to measure fast and slow fluctuations of labeled lysosomes and gain insight into lysosomal trafficking and metabolism [121].

A useful feature of RICS is the ability to create a high-resolution spatial diffusion map of the investigated macromolecule. The RICS technique can be implemented with cross-correlation (ccRICS) between two molecular species to investigate clustering of a kinase at the plasma membrane, degradation of exogenous DNA in cells, measure remodeling of adhesion complexes, and regulation of sub-apical trafficking of a phosphate cotransporter [122–129]. A modified version of RICS has been developed to minimize spectral cross-talk using statistical weighting of the signals [130].

The pixel size and dwell time must be compatible in order to implement RICS successfully [117, 124]. For example, scanning faster than the molecule's diffusion rate makes the species appear to be immobile. In contrast, the particle will diffuse away before being detected in subsequent pixels if scanning is performed at a rate slower than the characteristic diffusion of the molecule. Practically, pixel dwell times of 2–100 μsec and pixel sizes of 0.025–0.2 μm should be sufficient to measure the dynamics of a range of macromolecules. For example, a dwell time of 25 μs and pixel size ≤0.05 μm can measure the diffusion of a 25 kDa cytoplasmic protein by the second or third pixel scanned [115, 124]. Longfils et al. observed a 3–5-fold decrease in error on the diffusion constant by decreasing pixel size from 100 to 50 nm and they also observed consistent high quality RICS data over a board concentration range from nM to μM [131]. Minimum ROI of 2 μm × 2 μm is recommended by Brown et al. to prevent under-sampling. Overall, RICS is a powerful technique for measuring diffusion and complex dynamics across a range of timescales at the expense of a 2–3-fold lower resolution compared to FCS [124].

2.3.3 Image correlation spectroscopies

Image correlation spectroscopy (ICS), imaging cross-correlation spectroscopy (ICCS), spatiotemporal imaging correlation spectroscopy (STICS), and k-space imaging correlation spectroscopy (kICS) are additional methods that are imaging versions of FCS (for review see [132, 133]). All of these methods rely on

the acquisition of a time series of images from a confocal, two-photon, or TIR microscopy. The series of images amount to fluorescence intensity recorded as a function of time and space, $i(x,y,t)$, and the generalized spatiotemporal function is defined as

$$r_{ab}(\xi,,\eta,,\tau) = \frac{\delta i_a(x,,y,,t)\delta i_b(x+\xi,,y+\eta,,t+\tau)}{i_a(x,,y,,t)_t\, i_b(x,,y,,t+\tau)_{t+\tau}}$$

where the fluorescence fluctuation, $\delta i(x,,y,,t)$, is defined as $\delta i(x,,y,,t) = i(x,,y,,t) - i(x,,y,,t)_t$ [132]. This equation is for two different emission wavelength detection channels (a, b) and in the case of autocorrelation of one channel ($a = b$) the subscripts are dropped. The different ICS variants are just simplified versions of this equation for the specified limits. Importantly, all images acquired on the fluorescence microscope are a convolution of the emission of the fluorophore with the microscope's PSF. This convolution causes spreading of the diffraction limited fluorophore signal over several pixels in the image and this signal is correlated over space and time. This is a powerful technique because large numbers of stochastic fluctuations can be reduced to a small number of physically important parameters due to spatiotemporal averaging. An overriding assumption of ICS and related techniques are that the biological system being investigated is stationary in space, or time. This condition is not necessarily met in living systems such as cells that can move in space and time and are heterogeneous. In addition, conventional applications of these spatial imaging techniques are insensitive to interactions and molecular movements below the diffraction limit of ~200 nm. In the original ICS, the correlation function is calculated for each pixel from the raw data (images) and fitted to an analytical model to extract parameters such as cluster density and degree of aggregation of the molecular species is determined [134]. The amplitude peak of the calculated correlation is proportional to the number of particles. Broadening of the correlation peak can be caused by movement of the investigated particle and this initially limited ICS to the study of large clusters on the cell surface [135].

Srivastava et al. were able to enhance the ICS technique by extending into the time domain with temporal imaging correlation spectroscopy (TICS) [136]. The correlation function is calculated within and between images but only a single correlation function was calculated per image frame meaning there was no spatial, or vectoral information. Wiseman et al. combined ICS and TICS approaches to create spatiotemporal image correlation spectroscopy (STICS) [137, 138]. In this technique, there is dynamic and vectoral information encoded in the correlation peaks. In addition, sub-regions of samples could be quantified and velocity information determined. A two-color version of STICS was developed and given the name spatiotemporal image cross-correlation spectroscopy (STICCS) [139]. This technique was used to measure the cotransport of several integrin subtypes with paxillin and distinguish diffusion versus active transport [139]. A drawback to STICS and TICS is the potential photobleaching and dye photophysics (e.g. blinking) that can interfere with analysis [140].

A more recent variant of ICS is labeled k-space image correlation spectroscopy (kICS) and this technique utilizes 2D fast Fourier transformation to analyze the image data in the frequency domain (k-space ACF) [141]. Analyzing in k-space makes it easy to separate molecular dynamics from the artifactual photophysics of

the dye. An additional advantage of kICS is the dimensions of the PSF microscopy system are not needed for the analysis. In addition, complex mixtures of proteins undergoing directed transport and diffusion can be measured with kICS. The kICS technique has been used to study the transport dynamics of integrins and agonist induced clustering of CFTR in cholesterol microdomains [141, 142]. ICS and its modifications have been used with ~30–150 ms frame rates restricting these techniques to the study of large and slow-moving cellular structures on the cell surface and some intracellular organelles.

2.3.4 Number and brightness (N&B) analysis

Number and brightness (N&B) analysis, also known as scanning N&B, is a scanning extension to PCH, FIDA, and moment analyses developed by Digman et al. [143]. In this technique, the mean intensity and variance (i.e., 1st and 2nd moments) are calculated from each pixel of a series of images. The apparent brightness (B) of the molecule at each pixel can be calculated as the ratio of the variance to the average intensity (σ^2 / k). The number of mobile molecules (N) can be calculated as the ratio of total intensity to B (k^2 / σ^2) [143]. The parameter N is directly related to n particles. N&B analysis can be implemented using a confocal or widefield fluorescent microscope equipped with either point, or array detectors [143, 144]. It is important to correct for detector noise, background signal, and artifactual motion such as specimen drift or movement that can contribute to variance and lead to error [124, 145]. N&B analysis has been successfully implemented to measure oligomeric complexes in live cells such as remodeling of adhesion complexes, activation of ErbB receptors, Ebola viral capsid assembly, DNA and protein aggregation or oligomerization [79, 143, 146–151]. The cross-correlation N&B (ccN&B) approach extends N&B to two-colors and has been used to measure stoichiometric binding of focal adhesion and integrin protein complexes [116, 127, 152, 153].

Similar to RICS, it is important to select the proper pixel dwell time in order to capture the fluctuations. For example, a pixel dwell time of 25 μs is reasonable for a protein diffusing at ~20 $\mu m^2/s$ [143]. Autofluorescence, light scattering, and detector noise can all contribute to the signal variance, potentially contributing error to N&B analysis. Many times, these variances are independent and thus the "noise" is equal to the sum of the total variance [143]. Importantly, the variance due to the mobile molecules/species fluctuations will vary with the square of the brightness ($\sigma^2_n = \varepsilon^2 n$) resulting in a B value >1 and immobile species will have a B value of 1. A simple plot of variance as a function of intensity (increasing illumination) should lead to a quadratic relationship if the signal variance arises from the true molecular species and not "noise". Therefore, subtraction of 1 from the B value will give a true molecular brightness.

A limitation of N&B analysis, in its original form, was the inability to detect mixtures of several species in the same pixel and only weighted average brightness could be obtained.

Hortiguela et al. developed a statistical resampling of raw fluctuation data to measure coexisting oligomer species in each pixel and this improved N&B methodology is called enhanced N&B analysis (eN&B) [154, 155]. One drawback to eN&B is analysis requires 200 frames and can take from seconds to minutes to complete one timepoint. Overall, N&B analysis can robustly identify spatially heterogenous clusters of macromolecules in an image and generate a *spatiotemporal map of said clusters, but these are averaged values, unless eN&B is employed.*

2.3.5 Spatial intensity distribution analysis (SpIDA) and fluorescence intensity fluctuation (FIF) spectroscopy

Spatial intensity distribution analysis (SpIDA) was inspired by PCH analysis and creates fluorescence intensity histograms that are subsequently analyzed using super-Poissonian distribution functions [36]. In SpIDA, the density and quantal brightness (QB) of the fluorescently-labeled protein are calculated and can be used to determine expression level and oligomerization state. A given protein's QB can be compared to the QB of control proteins that are known to be monomer, or larger oligomers, therefore determining the oligomeric state of the protein of interest [36]. As a result, information regarding the densities of fluorescent molecules and their QB are obtained. While PCH is focused on the time domain, SpIDA is centered around the spatial domain of acquired images. The intensity histograms distributed from SpIDA analyses can elucidate the presence of dimers from monomers in a population based on intensity fluctuations, making this method of analysis beneficial in comparison to previous techniques discussed above. Importantly, the SpIDA technique is compatible with conventional immunostaining methods used on fixed cells and tissues that is a distinct advantage over PCH and N&B analyses [156]. SpIDA analysis software is freely available from the De Koninck lab (https://ydklab.org/tools). SpIDA analysis was employed to measure the QB and surface density of GPCR proteins in live and fixed cells. GPCRs or associated signaling proteins measured using the SpIDA approach include GABA(B) in spinal cord tissue, tyrosine kinase, secretin receptor, protein aggregation, and kinetics of fluorophore uptake in tissue culture cells [156–161].

Both N&B and eN&B fail to separate distinct oligomeric species based on brightness distribution. SpIDA can resolve multiple oligomeric species but at the expense of reduced resolution [44, 154, 162]. One and two-dimensional fluorescence intensity fluctuation (FIF) spectroscopy was developed to measure the effects of agonists and antagonists on the concentration, size, and stability of membrane receptor oligomers [162, 163]. Stoneman et al. were motivated to develop a rapid method that could accurately identify and measure mixtures of receptor oligomer sizes from individual pixels of images. Their technique requires the segmentation of a large ROI into hundreds of smaller ROIs (200–500 pixels) and thousands of concentration and brightness values are calculated from these ROIs. The brightness distributions calculated from the intensity fluctuations spread across the image pixels are used to generate spectrograms. The spectrograms, created for each segmented ROI, can then be used to measure the size and abundance of oligomeric species. The authors used FIF spectroscopy to probe the dynamic change in receptor oligomer size for the secretin (Class B GPCR) and epidermal growth factor receptors [162].

3. Advantages and disadvantages of FFTs

As mentioned above, clear advantages for FFTs include single molecule sensitivity, measurements at physiological concentrations, and high spatial, and temporal resolution. Protein complex stoichiometries and kinetics can also be measured with dual-color versions of FFTs. FFTs rely on fluorescence fluctuation measurements in space, time, or both to extract the molecular parameters. There are many factors that can affect the quality of the fluctuation data collected. Factors that can negatively impact FFT analysis include fluctuations not from the molecule of interest (i.e. cell movement, stage drift), fluorophore photobleaching, immobile species, illumination geometry artifacts, undesired photophysics of fluorophore, and detector characteristics [45, 164, 165].

The measurement time, or scan speed, must be appropriately matched with the macromolecule's diffusion rate in order to acquire sufficient fluctuations for analysis. It is also important to distinguish the molecule's fluctuation from other factors that can contribute to the signal variance. Slow cell or organelle movement can add additional fluctuations that create artifacts during analysis [88, 89, 164]. For example, Hennen et al. observed that a nuclear localized EGFP protein exhibited a concentration dependent increase of brightness [164]. The cytosolic version did not exhibit this unexpected behavior. After further analysis, they concluded that the anomalous result was due to movement of the nuclear membrane and employing MSQ corrected the problem. MSQ analysis was also used to correct for incomplete PSF overlap and photobleaching for measurements in bacteria [89]. Undulations affecting FFT measurements have been observed for other membranes and several strategies, including lowering the measurement temperature (22°C or 30°C instead of 37°C), algorithmic filtering of data, multiple short measurements, and removal of distorted correlation curves were employed to improve the analysis [166–169]. These extra-fluctuation effects can be problematic especially when sample thickness does not exceed the size of the observation volume. Finite sample thickness can lead to a bias in the brightness calculation but this can be corrected by performing an z-scan and using this data to better model the PSF shape when analyzing the FFT data [145, 170].

Photobleaching is more problematic for spot methods and less an issue for scanning FFTs and can lead to incorrect determination of molecular parameters. The two main approaches for correcting photobleaching are mathematical fitting of the experimental signal decay or moving average filters that do not rely on fitting [171]. Both mono- and bi-exponential functions have been applied to correct for the signal decay in FFT data with varying success [88, 168]. It can be difficult to correct using a fitting method because the decay rates can vary substantially from cell to cell [172]. Moving average filters, for imaging data, work by calculating the local average of each pixel in a time series (all images) and the average of the neighboring time-points (global) in the series. Next, the fluctuation at the local pixel is defined as the deviation from the local average and then the local pixel value is changed to the global average value plus the addition of the fluctuation value. The two methods for calculating the local average are called the box-car method, a.k.a. sliding window, and the exponential filtering method [143]. Filtering algorithms were applied to imaging FFT data to remove contributions from cellular movement or photobleaching and thus enhance the accuracy of the calculated molecular parameters [140, 143, 155, 173]. Lange et al. used a wavelet shrinking algorithm to reduce the false positive signal from 69% to 4% for the negative control in FCCS measurements [174]. Recently, Nolan et al. introduced the Robin Hood algorithm as an improved filtering method for live cell images with limited photon budget (i.e. low intensity signals) [175]. In this algorithm, counts are subtracted from high intensity images and then added to low intensity images in the series. The overall counts are preserved in the image series in contrast to the box-car or exponential methods where the filtering process can lead to loss of information because of the numerical processing (natural to real number).

FFT analysis can be negatively influenced by dead-time and afterpulse effects. The dead-time and afterpulse effects are intrinsic characteristics of detectors and can cause underestimation and overestimation of molecular brightness, as well as other molecular parameters (e.g. rotational diffusion), respectively [176, 177]. The dead-time of a detector is the fixed time after photon registration (e.g. 50 nanoseconds for actively quenched APD) where another event cannot be detected. If the signal intensity being measured is too great, or the temporal period is too short then a certain number of photons will not be registered leading to underestimation of ε.

The afterpulse effect is when there are additional spurious events registered after the real photon detection event and this leads to overestimation. For example, an APD can generate a nano- to microsecond delay that leads to a ~1% probability of detecting spurious events [176]. These two effects need to be corrected especially at higher concentrations [95, 177]. Hillesheim et al. conducted PCH measurements on a fluorescent dye in solution and calculated N and ε with or without correction for dead-time and afterpulse effects [177]. They found relative error >10% when there was more than one molecule present in the observation volume if corrections were not employed. One practical method to remove afterpulsing effects from FCS measurements is to split the signal being measured between two detectors and then calculate the cross-correlation (signal to self). Correlating the signal to itself can remove the spurious events and compensate for the afterpulsing effect. Importantly, individual detectors of the same brand, type, and make require fundamentally different mathematical models to correct for these effects and thus universal models cannot be generated and each detector must be characterized individually [178]. Fukushima et al. applied a two-detector approach to N&B analysis called TD-N&B to correct for detector artifacts when they measured the dynamics of glucocorticoid receptor dimerization [179].

The photophysics of the fluorescent dye, or protein can negatively influence the FFT analysis. For example, it is well known that a significant portion of certain fluorescent protein molecules do not properly mature and/or have long-lived triplet "dark" states (~10–70%) [180, 180–184]. These two processes can lead to a large number of molecules that do not fluorescence. In FCCS, if 100% of two labeled species are interacting then the CCF should be ideally 1.0, but in many experimental setups the value is ~0.5 which can lead to incorrect K_d determinations. Maturation problems, triplet state fraction, and photobleaching contribute to this discrepancy. The impact on FCCS analysis due to these effects can be corrected to provide label-independent K_d values [66, 180]. Correction factors can be employed to account for incomplete maturation of fluorescent proteins and this approach was used successfully to measure the oligomeric status of the homo-trimeric influenza A Hemagglutinin (HA) glycoprotein in live cells [183].

Overall, many of the disadvantages, or limitations of FFT measurements can be overcome with proper experimental design, and correction factors in the analytical models used to fit the data. It is important to thoroughly characterize your experimental setup, especially the detectors. Unfortunately, studying fast chemical processes necessitate the above-mentioned correction factors. Ideally, it is better to design experiments where the fluctuations being measured are not on the same time scale as the detector traits (i.e. dead-time, afterpulse) and that photobleaching, and other photophysical processes that have a negative impact, be minimized.

4. FFTs reveal new information on GPCR structure and function

Different GPCRs classes are known to vary in their oligomeric structure due to the varying propensity for dimerization and avidity of their interactions. Furthermore, agonist/antagonist ligands are known to alter GPCR quaternary structure. Generally speaking, the ability of GPCRs to associate with self, or other family members aligns with the receptor family. For example, class A GPCRs tend to transiently associate and multiple surfaces are required for the interaction [185]. In contrast, class C GPCRs form obligate dimers and higher-order oligomers [186]. While class B GPCRs appear to have an intermediate behavior to A and C receptors [187]. The class A family represent the largest class of GPCRs and it is heavily debated whether these receptors can form dimers, or larger structures due to

transient interactions [188]. The significance and molecular basis for these receptor complexes are poorly understood.

Historically, these GPCR oligomeric changes were observed using biochemical approaches such as Co-IP, FRET, BiFC, and BN-PAGE experiments. Often, different experimental approaches have yielded opposite conclusions concerning the oligomeric state of the GPCR. In the past decade, FFTs have been employed to measure the dynamics of GPCRs in live cells and these methods are revealing new insights into GPCR structure/function and may shed light onto the disparate results (**Table 2**).

Receptor name*	**Technique**	**Species observed (in the absence or presence of ligand)**	**References**
M1-muscarinic	FCS/PCH	Dimer	[82]
M2-muscarinic	FCS/PCH	Dimer	[82]
Serotonin (5-HT_{2A})	FCS/PCH	Dimer	[82]
Adrenergic (α_{1b}-AR)	FCS/PCH	Dimer	[82]
Adrenergic (β_2-AR)	FCS/PCH	Dimer	[82]
D1-Dopamine	FCS/PCH	Dimer	[82]
Serotonin (5-HT_{2C})	FCS/PCH	Dimer	[81, 83]
$GABA_{B1}$ & $GABA_{B2}$	SpIDA	Monomer/dimer	[157]
Secretin	SpIDA	Monomer/dimer	[160]
Secretin	2D-FIF	Monomer/dimer/higher-order oligomers	[162]
Neuropeptide Y	FCS	Clustering	[168]
D3-Dopamine	SpIDA	Monomer/dimer/higher-order oligomers	[193]
Serotonin (5-HT_{2C})	SpIDA	Monomer/dimer/higher-order oligomers	[194]
M1-Muscarinic	SpIDA	Monomer/dimer/higher-order oligomers	[197]
M3-Muscarinic	SpIDA	Monomer	[197]
μ-opioid	FCS/PCH/N&B	Tetramers/oligomers	[204]
δ-opioid	FCS/PCH	Tetramers/oligomers	[204]
A1-Adenosine & A2a-Adenosine	FCS	heterodimers	[205, 206]**
B2-Bradykinin	FCS/sFCS	Small/large aggregates	[207]
Complement (C5a)	FCS	Clusters	[208]

**GFP or YFP-tagged.*
***Fluorescent ligand used to label receptor.*

Table 2.
Summary of fluorescence fluctuation spectroscopy studies on GPCRs.

4.1 Muscarinic acetylcholine M_2 receptor: monomer, dimer, or tetramer?

One prominent example of controversy in the field is the quaternary state of the muscarinic acetylcholine M_2 receptor (M_2R). The M_2R was reported to be predominantly a monomer with capability to form dimers based on TIRF microscopy experiments in CHO cells, primary cardiac cells, and cardiac tissues [189]. In contrast, Herrick-Davis et al. reported M_2R was predominantly a dimer based on FCS/PCH analysis in transfected cell lines [82], while FRET, single molecule photobleaching (smPB), and ligand binding assays yielded results consistent with

a tetrameric arrangement for M_2R [190, 191]. What factors could account for these seemingly contradictory results?

Recent biochemical studies on three distinct class A GPCRs using proteoliposomes reported that environmental factors, including membrane curvature and receptor density, affect degree of homo-oligomerization [192]. A concentration dependent increase in the number and complexity of oligomeric species has been observed for both the 5-HT2C and dopamine D3 receptors (D_3R) based on SpIDA analyses [193, 194]. In addition, the experimental temperature used can have a profound impact on the GPCR being investigated. Nenasheva et al. observed a two-fold change in mobility for every 10°C change in temperature, suggesting alterations in protein-protein interactions or protein-lipid interactions or both [189].

Expression level differences between the smPB and FCS experiments for M_2R seem unlikely given there were ~880,000 receptors per cell and ~52,000–620,000 receptors per cell, respectively [82, 195]. These levels of expression are within an order of magnitude for M_2R in rat cardiomyocytes that are estimated at 1.7×10^6 copies per cell [196]. The discrepancies in the M_2R results could be explained by photobleaching in the FCS/PCH measurements. It is well known that slow moving membrane proteins are prone to photobleaching during FCS measurements and photobleaching "shortens" the apparent diffusion time of the species [45, 79, 165]. Photobleaching can be difficult to detect because fluorescent molecules replenish the bleached molecules leading to a steady intensity recording that does not decrease with time as expected. Stavesich et al. refer to this scenario as "cryptic" bleaching [165]. Therefore, it is possible that slower moving, and/or immobile tetrameric species were not "visible" in the FCS experiments but were in the FRET and single-particle experiments. The authors acknowledge that less mobile GPCR clusters in membrane microdomains would not be detectable in their FCS/PCH analysis [82].

4.2 SpIDA analyses of GPCR organization and dynamics

Many FFT studies performed to date have utilized the SpIDA technique to measure mEGFP-tagged GPCR proteins [36, 160, 188, 193, 194]. The original studies that employed SpIDA measured the organization of $GABA_{B1}$ and $GABA_{B2}$ receptors alone and in combination through antibody staining in rat spinal cords [157]. Godin et al. demonstrated through single- and double-labeling of B_1 and B_2 receptors that SpIDA returned the expected oligomerization state of monomer (single label) and dimer (double label). The authors also measured the dynamics of EGFR-GFP in absence and presence of 20 nM EGF [157]. Short-term incubation with EGF increased the amount of dimeric EGFR-GFP without any change in total protein on the surface suggesting that changes in monomer levels were not due to receptor internalization. These measurements were performed on a range of expression levels from 100,000 to 600,000 receptors/cell (32–220 EGFR per μm^2) suggesting the oligomeric changes seen are not concentration dependent.

Milligan et al. measured 5-HT2C in the absence and presence of several distinct chemical ligands. They observed mostly monomeric 5-HT2C at low expression levels and a concentration dependent increase to larger oligomeric sizes. Several antagonists, including SB221284, disrupted the larger oligomeric species into monomers and this was a time-dependent effect that was reversible by washing out the chemical [194]. Similar observations were seen for D_3R where increased receptor expression in the plasma membrane shifted the receptor organization to dimer and higher-order oligomers [193]. Interestingly, several antagonists, including spiperone and haloperidol, promoted monomerization of the D_3R while others, such as

eticlopride, nemonapide, and clozapine, had no effect. Importantly, Marsango et al. created a mutated version of D_3R ($Asp_{110}Ala$) that reduced its affinity for spiperone and this mutant receptor had less conversion to monomer species in the presence of ligand. This result suggests that the ligand affects the receptor-receptor interactions and not the lipid membrane, or another associated protein. Molecular dynamic simulations suggested that that spiperone binding increased the distance between transmembrane IV-V and haloperidol binding increased the distance between transmembrane I-II, which could disrupt interactions [193].

Measurements of the muscarinic M_1 receptor using SpIDA revealed mostly monomer organization in the basal state with some dimers/larger species (75:25 ratio) and addition of the antagonist pirenzepine caused a large shift to larger species (73.5%) [197]. Importantly, sustained treatment with pirenzepine also caused increase receptor expression from ~50 to ~120 receptor copies per μm^2. Unfortunately, the authors were not able to determine if the shift to larger species upon antagonist incubation was due to binding, or increased expression. Similar to D_3R, other antagonists had no effect on receptor association, such as the non-selective agents' atropine and *N*-methylscopolamine [197]. Disruption of the actin cytoskeleton with cytochalasin D enhanced M_1 receptor oligomerization and this is not surprising given, cytochalasin D is known to redistribute caveolar/lipid raft-resident proteins, including GPCRs (β_1-adrenergic receptors (β_1-AR, β_2-AR)), and increase cAMP levels [198]. The enhanced M_1 receptor oligomerization was most likely caused by altered interactions of the GPCR with adenylate cyclase and $G\alpha_s$ due to disruption of lipid rafts/caveolae [198]. In contrast, the M_3 receptor quaternary organization was not affected upon incubation with either pirenzepine or telenzepine antagonists [197]. Interestingly, the M_3 receptor was measured as mostly monomers (~80%) based on SpiDA analysis but FRET analysis suggested the receptor existed as a mixture of dimers and tetramers [197, 199]. It is important to note that for the FRET study M_3 receptor-Citrine and M_3-receptor-Y149C/A239-Cerulean were co-expressed and used for measurements. The Y149C/A239 mutation alters receptor ligand selectivity to allow activation by a synthetic chemical instead of acetylcholine [200]. The FRET study does not appear to have used monomeric versions of Citrine and Cerulean unlike the SpIDA study (mEGFP) and this could have led to oligomerization artifacts [201].

Most FFT studies on GPCRs have focused on class A receptors but two recent studies were performed on the peptide hormone secretin receptor (class B). Ward et al. observed a mixed population of monomers (33.8%) and dimers (59.2%) with only a small portion of receptors forming higher-order oligomers (7.1%) based on SpIDA analysis [160]. Addition of sodium butyrate, known to increase expression of GPCRs from viral promoters, led to increased expression and formation of higher-order oligomers (22% versus 7.1%) [160, 202]. Mutation of residues Gly^{243} and lle^{247} to Ala in the lipid-facing side of transmembrane IV disrupted secretin receptor oligomerization, reduced cAMP production but did not change ligand binding affinity to the receptor [203]. SpIDA analysis indicated this mutant receptor was 90% monomeric and there was no change in receptor association upon sodium butyrate addition. Interestingly, cholera toxin inhibition of $G\alpha_s$ expression in cells did not affect secretin oligomerization, suggesting receptor protein-protein interactions mediate dimer formation [160]. Short-term incubation of the mutant secretin receptor with secretin caused an increase in dimeric population but the wildtype receptor organization remained unchanged. It is known that the receptor can be internalized as a monomer, and the authors hypothesize that the increase in dimer formation could be due to clathrin-mediated clustering instead of genuine receptor-receptor interaction, but this remains to be determined.

4.3 FCS, PCH, and N&B analyses of GPCR organization and dynamics

In addition to SpIDA studies, FCS, PCH and N&B analyses have been used to probe the dynamic assembly/disassembly of GPCRs [81–83, 168, 204–208]. Golebiewska et al. measured the oligomeric assembly of opioid receptor (OR) complexes in Neuro-2a cells [204]. They observed eYFP-μOR diffused in the plasma membrane at a rate of 7.3×10^{-9} cm^2/sec suggesting the receptor is organized as dimers and tetramers based on FCS measurements. This diffusion rate was not affected upon incubation with 1 μM morphine ligand for 24 hours. However, co-expression of eYFP-μOR or eGFP-μOR with unlabeled μOR led to a decrease in the diffusion rate suggesting the formation of higher order oligomers. Moreover, incubation with a range of morphine concentrations over 24 hours significantly increased diffusion in a dose-dependent manner and this effect was reversible upon co-incubation with the antagonist naloxone. These results suggested that morphine disrupted the OR complexes into smaller species. In contrast to the FCS results, the eGFP-μOR molecular brightness increased (dimers to tetramers) in the presence of morphine based on N&B analysis. Furthermore, co-expression of eGFP-μOR with unlabeled μOR had a molecular brightness the same as eGFP-μOR alone but with a greatly reduced diffusion rate. The simplest model to explain this result was if two eGFP-μOR are in complex with two μOR forming a mixed tetramer of labeled and unlabeled receptors. Importantly, the brightness values for these complexes was broad which could mean there was anywhere from one to three eGFP-μOR. Their FFT measurements coincided with the results they obtained from FRET.

Pharmacological modulation of adenosine receptor function can be used to treat heart arrhythmias, asthma, stroke, and renal failure [209]. Adenosine A_1 and A_{2a} heterodimers displayed a faster diffusion rate in the plasma membrane of CHO cells compared to homodimers (5.6×10^{-9} versus 4.0×10^{-9} cm^2/sec) based on FCS experiments [205]. Briddon et al. used a fluorescently labeled A_1 agonist to quantify binding to the adenosine A_1 receptor in single cells [206]. They identified at least two populations of receptors with varying diffusion times (tens to hundreds of millisecond) upon incubation with the agonist [206, 210]. Furthermore, there was a reduction in the amount of receptor complexes in the presence of an antagonist suggesting disruption of oligomer formation.

Bradykinin receptors (subtype B1 and B2) are GPCRs that mediate vascular contribution to inflammation and edema [211]. Single point and scanning FCS were used to measure the mobility of bradykinin subtype B2 receptor-GFP (B_2R-GFP) expressed in HEK293 cells [207]. The B_2R-GFP diffusion rate was measured to be 3.5×10^{-9} cm^2/sec in the plasma membrane by single point FCS and a similar rate was observed whether one- or two-photon microscopy was employed. Scanning FCS identified three populations of receptor with a large portion (~72%) of receptors located in slow-moving aggregates. The FCS results combined with binding studies and FRET suggested that B_2R complexes are dynamic and that pre-formed receptor-G protein complexes initiate rapid signaling through a limited number of molecules.

BiFC was combined with FCS analysis to identify and measure complex dynamics between the neuropeptide Y (NPY) receptor and β-arrestin [168]. The NPY receptors play critical roles in food intake, bone metabolism, and cardiovascular regulation [212]. Y1 and Y2 receptors were measured to have similar diffusion rates ~2.0×10^{-9} cm^2/sec and treatment with NPY to cause internalization decreased the diffusion rate of Y1-GFP receptor but not Y2-GFP receptor. Mutations in β-arrestin that prevented recruitment and internalization blocked the agonist induced diffusion changes observed for Y1-receptor. NPY treatment of Y1-receptor also caused an increase in brightness (~1.5 fold) based on PCH measurements suggesting

receptor clustering. Overall, Kilpatrick et al. interpreted their results to mean they were observing early events in arrestin dependent clustering and endocytosis of Y1-receptor. An important observation in this study was in relation to one of their control proteins used for PCH analysis. The authors used a membrane anchored GAP-GFP and were surprised to find the brightness of it was the same as Y1-GFP which they measured as a dimer based on FRET. They noted that the concentration level for GAP-GFP in the plasma membrane was 0.05 mM based on FCS. This concentration is very close to the K_d (0.1 mM) measured for GFP *in vitro* [213]. Their conclusion was that their membrane embedded monomeric control was probably clustering as a dimer possibly due to lipid microdomains.

4.4 Experimental caveats of FFT measurements on GPCRs

Most FFTs are ensemble measurements that report an average of the population compared to single particle experiments that focus on a single molecule and this should be kept in mind when trying to compare FFTs to single particle tracking experiments. It is very important to confirm that monomeric and dimeric controls for FFT measurements are appropriate for the analysis. Controls used in the above discussed studies included roundabout receptor 1 (dimeric axonal guidance receptor), EGFR (dimeric), CD-86 (monomeric), CD-28 (dimeric), GABA heterodimer, palmitoylated-mEGFP (PM1) and palmitoylated-myristoylated-mEGFP-mEGFP (PM2) [82, 160, 162, 214]. For fixed cells/tissues, samples stained with secondary antibody only or background staining outside cells (primary and secondary) were assumed to have a nonspecific and monomeric distribution for the fluorescence signal [157]. Confirmation using a complimentary biochemical (e.g. blue native gel, column chromatography) approach to confirm oligomeric status of the control would be helpful. In addition, maintaining reasonable expression levels (lower than K_d, if known) to prevent non-specific interaction of control proteins is critical for proper calibration and determination of number of receptor subunits.

Many FFT studies chose to measure the receptor at lower temperatures (22–23°C) to minimize cellular movements and this should be kept in mind when interpreting dynamics that are not at a physiologically relevant temperature. SpIDA measurements for 5-HT2C, D_3R, M_1 receptor, M_3 receptor and secretin receptor were performed on the basolateral/ventral surface of cells [83, 193, 194, 197]. Receptor organization appears to vary depending on the membrane region measured. For example, 5-HT2C receptor measured at the apical surface of choroid plexus epithelial tissue (32 receptors/μm^2) and dorsal surface of HEK293 cells are dimeric (~30 receptors/μm^2) but at the basolateral/ventral surface is mostly monomeric (50 receptors/μm^2) when measured at similar receptor densities [83, 194].

What factors besides technical shortcomings/artifacts could account for the observed differences in the oligomeric structure of 5-HT2C receptor? Oligomeric differences could be due to organizational differences in cytoskeletal and associated membrane proteins and/or differences in membrane tension [215, 216]. Clathrin forms membrane invaginations (pits) during endocytosis but can also form flat lattice sheets (FLCs) and the amount of lattice sheets can vary up to two-fold higher on the ventral versus dorsal membrane for HeLa and HEK293 cells [215]. Quantitative super-resolution imaging suggests that FLCs can functionally compartmentalize the plasma membrane to regulate signaling and FLCs can recruit or exclude the GCPR chemokine receptor 5 (CCR5). The interactions between CCR5 and FLCs can be long-lived (minutes up to an hour) upon agonist stimulation independent of endocytosis [215]. Furthermore, lipid composition, curvature and membrane tension can affect GPCR oligomerization partly driven by receptor-membrane hydrophobic matching [217, 218]. Importantly, membrane tension is

~4 times greater in regions that are connected to the cytoskeleton versus those that are not and affects clathrin assembly [219, 220]. The proportional contributions of these various processes could vary in the different membrane domains (dorsal versus ventral) of the cell leading to alteration in GPCR oligomerization.

Recently, there is a debate over the size and location of ROI to be taken for certain image FFTs such as SpIDA and 2D-FIF [163, 221, 222]. This debate stems from what one considers to be a biologically-relevant length scale. Annibale and Lohse suggested the implementation of an additional step in 2D-FIF protocol that includes case-by-case selection of homogenous regions of the membrane in order to exclude fluorescence "hotspots" [221]. It is not surprising to observe heterogeneities of image data as one "zooms" in given the compartmentalization of the plasma membrane due to cortical actin and clathrin structures [215, 223]. Their reasoning for this modification is that hotspots occur due to sub-cellular structures and/or artifacts unrelated to receptor oligomerization, adding to the heterogeneity of data, thus confounding the analysis. Stoneman et al. responded to Annibale and Lohse's concerns by pointing out that the brightness heterogeneity (~1.5) observed in their ROI sampling falls within the distribution of their monomeric control. This result implies two symmetrical data points exist 1.5 above and below the center of the Gaussian peak for the distribution that would represent 0.5 monomer [163]. Clearly, 0.5 of a monomer is not possible and this variation can be partly explained by micro-environment of fluorophore, fluorophore orientation with respect to polarization of excitation light and three dimensional folds of membrane [163]. Stoneman et al. do acknowledge that brightness fluctuations of 2-fold or greater are needed for the brightness spectrums to identify larger oligomeric species. They also emphasize that 2D-FIF inherently employs a rigorous low-pass filter during generation of spectrogram to remove the contribution from "hotpsots" and this is less subjective then manual selection. The Annibale's brightness values (supplemental Table 1, [163]) using Stoneman's data do not agree with Stoneman's original published work and current re-analyses [162, 163, 221]. Stoneman suggests that this could be due to a flaw in their analysis procedure (i.e. correction for detector variance and intensity background). There is also disagreement concerning whether SpIDA and 2D-FIF fail to discriminate large oligomers from large immobile background spots. Finally, both Stoneman and Annibale agree that combining spatial and temporal information (e.g. N&B approach with FIF) would be a robust approach. Overall, FFTs are powerful tools to measure dynamic changes in GPCRs organization in their native membrane environment provided the microscopic system is thoroughly characterized, appropriate controls are employed, sufficient number/size of ROI is measured and careful analysis performed.

5. Conclusions

GPCRs are dynamic receptors that can form transient homo- and hetero-oligomers, and alteration in receptor quaternary states can impact signaling ability. Recent FFT experiments have shed new light on the affect agonists, antagonists, and ligands have on the oligomeric status of several class A and one class B receptor. These fluorescence fluctuation analyses provide complimentary information to the more traditional biochemical, FRET, and radioligand studies performed on GPCRs. The power of these analyses is the ability to measure receptor dynamics at microsecond time scales on a few molecules with micrometer spatial resolution. Unfortunately, there is still controversy and disagreement on the oligomeric status of many GPCRs when comparing previous results to the more recent SpIDA, FCS, PCH, and N&B data. Some of the discrepancies could be contributed to

measurement location in cell membrane, or experimental conditions (e.g. different temperature, photobleaching). Other likely contributors to these differences are the limitations of measuring ensembles of molecules versus single particle tracking and the spatial/temporal scales of the different techniques. Researchers are beginning to combine multiple techniques such as FFTs with super-resolution or other biochemical approaches (BiFC-FCS) to compensate for individual shortcomings. Application of these combined approaches to study GPCR dynamics not just in the plasma membrane but other internal organelles in cells and live animal tissues will hopefully help to resolve conflicting experimental results.

Acknowledgements

Our sincere thanks to Dr. Amanda Storm for proofreading our manuscript, and our apologies to the authors whose research we were unable to cite due to page constraints.

Author details

Robert T. Youker* and Danielle Voet
Department of Biology, Western Carolina University, Cullowhee, North Carolina, USA

*Address all correspondence to: rtyouker@wcu.edu

References

[1] Calebiro D, Godbole A. Internalization of G-protein-coupled receptors: Implication in receptor function, physiology and diseases. Best Practice & Research Clinical Endocrinology & Metabolism. 2018;**32**:83-91

[2] Fredriksson R, Schiöth HB. The repertoire of G-protein–coupled receptors in fully sequenced genomes. Molecular Pharmacology. 2005;**67**:1414-1425

[3] Fredriksson R, Lagerström MC, Lundin L-G, et al. The G-protein-coupled receptors in the human genome form five main families. Phylogenetic analysis, paralogon groups, and fingerprints. Molecular Pharmacology. 2003;**63**:1256-1272

[4] Gurevich VV, Gurevich EV. The structural basis of arrestin-mediated regulation of G-protein-coupled receptors. Pharmacology & Therapeutics. 2006;**110**:465-502

[5] de Mendoza A, Sebé-Pedrós A, Ruiz-Trillo I. The evolution of the GPCR signaling system in eukaryotes: Modularity, conservation, and the transition to metazoan multicellularity. Genome Biology and Evolution. 2014;**6**:606-619

[6] Derelle R, Lopez P, Guyader HL, et al. Homeodomain proteins belong to the ancestral molecular toolkit of eukaryotes: Evolution of homeodomains. Evolution & Development. 2007;**9**:212-219

[7] Fritz-Laylin LK, Prochnik SE, Ginger ML, et al. The genome of *Naegleria gruberi* illuminates early eukaryotic versatility. Cell. 2010;**140**:631-642

[8] Wickstead B, Gull K, Richards TA. Patterns of kinesin evolution reveal a complex ancestral eukaryote with a multifunctional cytoskeleton. BMC Evolutionary Biology. 2010;**10**:110

[9] Grau-Bové X, Sebé-Pedrós A, Ruiz-Trillo I. A genomic survey of HECT ubiquitin ligases in eukaryotes reveals independent expansions of the HECT system in several lineages. Genome Biology and Evolution. 2013;**5**:833-847

[10] Lagerström MC, Schiöth HB. Structural diversity of G protein-coupled receptors and significance for drug discovery. Nature Reviews Drug Discovery. 2008;**7**:339-357

[11] Hu G-M, Mai T-L, Chen C-M. Visualizing the GPCR network: Classification and evolution. Scientific Reports. December 2017;**7**:1-15, 15495. DOI: 10.1038/s41598-017-15707-9. [Epub ahead of print]

[12] Strotmann R, Schröck K, Böselt I, et al. Evolution of GPCR: Change and continuity. Molecular and Cellular Endocrinology. 2011;**331**:170-178

[13] Attwood TK. A compendium of specific motifs for diagnosing GPCR subtypes. Trends in Pharmacological Sciences. 2001;**22**:162-165

[14] Horn F. GPCRDB information system for G protein-coupled receptors. Nucleic Acids Research. 2003;**31**:294-297

[15] Sgourakis NG, Bagos PG, Papasaikas PK, et al. A method for the prediction of GPCRs coupling specificity to G-proteins using refined profile hidden Markov models. BMC Bioinformatics. 2005;**6**:104

[16] Nordstrom KJV, Sallman Almen M, Edstam MM, et al. Independent HHsearch, Needleman-Wunsch-based, and motif analyses reveal the overall hierarchy for most of the G protein-coupled receptor families.

Molecular Biology and Evolution. 2011;**28**:2471-2480

[17] Pandey S, Assmann SM. The Arabidopsis putative G protein–coupled receptor GCR1 interacts with the G protein α subunit GPA1 and regulates abscisic acid signaling. The Plant Cell. 2004;**16**:1616-1632

[18] Krishnan A, Almén MS, Fredriksson R, et al. The origin of GPCRs: Identification of mammalian like rhodopsin, adhesion, glutamate and frizzled GPCRs in fungi. PLoS One. 2012;**7**:e29817

[19] Sriram K, Insel PA. G protein-coupled receptors as targets for approved drugs: How many targets and how many drugs? Molecular Pharmacology. 2018;**93**:251-258

[20] Hauser AS, Attwood MM, Rask-Andersen M, et al. Trends in GPCR drug discovery: New agents, targets and indications. Nature Reviews Drug Discovery. 2017;**16**:829-842

[21] Pándy-Szekeres G, Munk C, Tsonkov TM, et al. GPCRdb in 2018: Adding GPCR structure models and ligands. Nucleic Acids Research. 2018;**46**:D440-D446

[22] Hanlon CD, Andrew DJ. Outside-in signaling—A brief review of GPCR signaling with a focus on the Drosophila GPCR family. Journal of Cell Science. 2015;**128**:3533-3542

[23] Pitcher JA, Freedman NJ, Lefkowitz RJ. G protein–coupled receptor kinases. Annual Review of Biochemistry. 1998;**67**:653-692

[24] Luttrell LM, Ferguson SSG, Daaka Y, et al. β-Arrestin-dependent formation of β_2 adrenergic receptor-Src protein kinase complexes. Science. 1999;**283**:655-661

[25] Palczewski K, Buczyłko J, Kaplan MW, et al. Mechanism of rhodopsin kinase activation. The Journal of Biological Chemistry. 1991;**266**:12949-12955

[26] Jong Y-JI, Harmon SK, O'Malley KL. Intracellular GPCRs play key roles in synaptic plasticity. ACS Chemical Neuroscience. 2018;**9**:2162-2172

[27] Eichel K, von Zastrow M. Subcellular organization of GPCR signaling. Trends in Pharmacological Sciences. 2018;**39**:200-208

[28] Liggett SB. Phosphorylation barcoding as a mechanism of directing GPCR signaling. Science Signaling. 2011;**4**:pe36-pe36

[29] Shenoy SK, Lefkowitz RJ. β-Arrestin-mediated receptor trafficking and signal transduction. Trends in Pharmacological Sciences. 2011;**32**:521-533

[30] Charest PG, Oligny-Longpré G, Bonin H, et al. The V2 vasopressin receptor stimulates ERK1/2 activity independently of heterotrimeric G protein signalling. Cellular Signalling. 2007;**19**:32-41

[31] McDonald PH, Chow CW, Miller WE, et al. Beta-arrestin 2: A receptor-regulated MAPK scaffold for the activation of JNK3. Science. 2000;**290**:1574-1577

[32] DeFea KA, Zalevsky J, Thoma MS, et al. β-Arrestin–dependent endocytosis of proteinase-activated receptor 2 is required for intracellular targeting of activated Erk1/2. Journal of Cell Biology. 2000;**148**:1267-1282

[33] Steen A, Larsen O, Thiele S, et al. Biased and G protein-independent signaling of chemokine receptors. Frontiers in Immunology. 23 June 2014;**5**(277):1-13. Article ID: 277. DOI: 10.3389/fimmu.2014.00277. [Epub ahead of print]

[34] Vischer HF, Watts AO, Nijmeijer S, et al. G protein-coupled receptors:

Walking hand-in-hand, talking hand-in-hand?: GPCR oligomerization and crosstalk. British Journal of Pharmacology. 2011;**163**:246-260

[35] Inoue A, Raimondi F, Kadji FMN, et al. Illuminating G-protein-coupling selectivity of GPCRs. Cell. 2019;**177**:1933-1947.e25

[36] Pediani JD, Ward RJ, Marsango S, et al. Spatial intensity distribution analysis: Studies of G protein-coupled receptor oligomerisation. Trends in Pharmacological Sciences. 2018;**39**:175-186

[37] Ward RJ, Milligan G. Structural and biophysical characterisation of G protein-coupled receptor ligand binding using resonance energy transfer and fluorescent labelling techniques. Biochimica et Biophysica Acta (BBA) - Biomembranes. 2014;**1838**:3-14

[38] Guo H, An S, Ward R, et al. Methods used to study the oligomeric structure of G-protein-coupled receptors. Bioscience Reports. 30 April 2017;**37**:1-19. DOI: 10.1042/BSR20160547. [Epub ahead of print]

[39] Cottet M, Faklaris O, Maurel D, et al. BRET and time-resolved FRET strategy to study GPCR oligomerization: From cell lines toward native tissues. Frontiers in Endocrinology. 2012;**3**(92):1-14. Article ID: 92. DOI: 10.3389/fendo.2012.00092. [Epub ahead of print]

[40] Shimada I, Ueda T, Kofuku Y, et al. GPCR drug discovery: Integrating solution NMR data with crystal and cryo-EM structures. Nature Reviews Drug Discovery. 2019;**18**:59-82

[41] Weidemann T, Mücksch J, Schwille P. Fluorescence fluctuation microscopy: A diversified arsenal of methods to investigate molecular dynamics inside cells. Current Opinion in Structural Biology. 2014;**28**:69-76

[42] González Bardeci N, Angiolini JF, De Rossi MC, et al. Dynamics of intracellular processes in live-cell systems unveiled by fluorescence correlation microscopy: FCS in biological studies. IUBMB Life. 2017;**69**:8-15

[43] Youker RT. Detectors for super-resolution & single-molecule fluorescence microscopies. In: Britun N, Nikiforov A, editors. Photon Counting—Fundamentals and Applications. Rijkea, Croatia: InTech; 21 March 2018. DOI: 10.5772/intechopen.71943. [Epub ahead of print]

[44] Bag N, Wohland T. Imaging fluorescence fluctuation spectroscopy: New tools for quantitative bioimaging. Annual Review of Physical Chemistry. 2014;**65**:225-248

[45] Youker RT, Teng H. Measuring protein dynamics in live cells: Protocols and practical considerations for fluorescence fluctuation microscopy. Journal of Biomedical Optics. 2014;**19**:090801

[46] Gunther G, Jameson DM, Aguilar J, et al. Scanning fluorescence correlation spectroscopy comes full circle. Methods. 2018;**140-141**:52-61

[47] Magde D, Elson E, Webb WW. Thermodynamic fluctuations in a reacting system—Measurement by fluorescence correlation spectroscopy. Physical Review Letters. 1972;**29**:705-708

[48] Ehrenberg M, Rigler R. Rotational brownian motion and fluorescence intensify fluctuations. Chemical Physics. 1974;**4**:390-401

[49] Schwille P, Kummer S, Heikal AA, et al. Fluorescence correlation spectroscopy reveals fast optical excitation-driven intramolecular

dynamics of yellow fluorescent proteins. Proceedings of the National Academy of Sciences. 2000;**97**:151-156

[50] Schwille P, Haupts U, Maiti S, et al. Molecular dynamics in living cells observed by fluorescence correlation spectroscopy with one- and two-photon excitation. Biophysical Journal. 1999;**77**:2251-2265

[51] Briddon SJ, Kilpatrick LE, Hill SJ. Studying GPCR pharmacology in membrane microdomains: Fluorescence correlation spectroscopy comes of age. Trends in Pharmacological Sciences. 2018;**39**:158-174

[52] Rat V, Pinson X, Seigneuret F, et al. Hepatitis B virus core protein domains essential for viral capsid assembly in a cellular context. Journal of Molecular Biology. May 2020;**432**(13):3802-3819. DOI: 10.1016/j.jmb.2020.04.026. [Epub ahead of print]

[53] Fujita H, Oikawa R, Hayakawa M, et al. Quantification of native mRNA dynamics in living neurons using fluorescence correlation spectroscopy and reduction-triggered fluorescent probes. Journal of Biological Chemistry. 2020;**295**(23):7923-7940

[54] Fukuda T, Kawai-Noma S, Pack C-G, et al. Large-scale analysis of diffusional dynamics of proteins in living yeast cells using fluorescence correlation spectroscopy. Biochemical and Biophysical Research Communications. 2019;**520**:237-242

[55] Nomura Y, Nakamura T, Feng Z, et al. Direct quantification of gene expression using fluorescence correlation spectroscopy. Current Pharmaceutical Biotechnology. 2007;**8**:286-290

[56] Betaneli V, Mücksch J, Schwille P. Fluorescence correlation spectroscopy to examine protein–lipid interactions in membranes. In: Kleinschmidt JH, editor. Lipid-Protein Interactions. New York, NY: Springer New York. 2019. pp. 415-447

[57] Vasconcelos L, Lehto T, Madani F, et al. Simultaneous membrane interaction of amphipathic peptide monomers, self-aggregates and cargo complexes detected by fluorescence correlation spectroscopy. Biochimica et Biophysica Acta (BBA) - Biomembranes. 2018;**1860**:491-504

[58] Wohland T, Friedrich K, Hovius R, et al. Study of ligand–receptor interactions by fluorescence correlation spectroscopy with different fluorophores: Evidence that the homopentameric 5-hydroxytryptamine type 3 $_{As}$ receptor binds only one ligand †. Biochemistry. 1999;**38**:8671-8681

[59] Jakobs D, Sorkalla T, Haberlein H. Ligands for fluorescence correlation spectroscopy on G protein-coupled receptors. Current Medicinal Chemistry. 2012;**19**:4722-4730

[60] Zemanová L, Schenk A, Hunt N, et al. Endothelin receptor in virus-like particles: Ligand binding observed by fluorescence fluctuation spectroscopy. Biochemistry. 2004;**43**:9021-9028

[61] Maeder CI, Hink MA, Kinkhabwala A, et al. Spatial regulation of Fus3 MAP kinase activity through a reaction-diffusion mechanism in yeast pheromone signalling. Nature Cell Biology. 2007;**9**:1319-1326

[62] Slaughter BD, Schwartz JW, Li R. Mapping dynamic protein interactions in MAP kinase signaling using live-cell fluorescence fluctuation spectroscopy and imaging. Proceedings of the National Academy of Sciences. 2007;**104**:20320-20325

[63] Tiwari M, Oasa S, Yamamoto J, et al. A quantitative study of internal and

external interactions of homodimeric glucocorticoid receptor using fluorescence cross-correlation spectroscopy in a live cell. Scientific Reports. December 2017;**7**:1-16. Article ID: 4336. DOI: 10.1038/s41598-017-04499-7. [Epub ahead of print]

[64] Jastrzebska B, Comar WD, Kaliszewski MJ, et al. A G protein-coupled receptor dimerization Interface in human cone opsins. Biochemistry. 2017;**56**:61-72

[65] Teichmann A, Gibert A, Lampe A, et al. The specific monomer/dimer equilibrium of the corticotropin-releasing factor receptor type 1 is established in the endoplasmic reticulum. Journal of Biological Chemistry. 2014;**289**:24250-24262

[66] Kaliszewski MJ, Shi X, Hou Y, et al. Quantifying membrane protein oligomerization with fluorescence cross-correlation spectroscopy. Methods. 2018;**140-141**:40-51

[67] Chen J, Nag S, Vidi P-A, et al. Single molecule in vivo analysis of toll-like receptor 9 and CpG DNA interaction. PLoS One. 2011;**6**:e17991

[68] Li Y, Shivnaraine RV, Huang F, et al. Ligand-induced coupling between oligomers of the M2 receptor and the Gi1 protein in live cells. Biophysical Journal. 2018;**115**:881-895

[69] Rogacki MK, Golfetto O, Tobin SJ, et al. Dynamic lateral organization of opioid receptors (kappa, mu_{wt} and mu_{N40D}) in the plasma membrane at the nanoscale level. Traffic. 2018;**19**:690-709

[70] Meseth U, Wohland T, Rigler R, et al. Resolution of fluorescence correlation measurements. Biophysical Journal. 1999;**76**:1619-1631

[71] Chen Y, Müller JD, So PTC, et al. The photon counting histogram in fluorescence fluctuation spectroscopy. Biophysical Journal. 1999;**77**:553-567

[72] Kask P, Palo K, Ullmann D, et al. Fluorescence-intensity distribution analysis and its application in biomolecular detection technology. Proceedings of the National Academy of Sciences. 1999;**96**:13756-13761

[73] Kask P, Palo K, Fay N, et al. Two-dimensional fluorescence intensity distribution analysis: Theory and applications. Biophysical Journal. 2000;**78**:1703-1713

[74] Müller JD, Chen Y, Gratton E. Resolving heterogeneity on the single molecular level with the photon-counting histogram. Biophysical Journal. 2000;**78**:474-486

[75] Yu L, Tan M, Ho B, et al. Determination of critical micelle concentrations and aggregation numbers by fluorescence correlation spectroscopy: Aggregation of a lipopolysaccharide. Analytica Chimica Acta. 2006;**556**:216-225

[76] Meng F, Ma H. A comparison between photon counting histogram and fluorescence intensity distribution analysis. The Journal of Physical Chemistry B. 2006;**110**:25716-25720

[77] Saffarian S, Li Y, Elson EL, et al. Oligomerization of the EGF receptor investigated by live cell fluorescence intensity distribution analysis. Biophysical Journal. 2007;**93**:1021-1031

[78] Slaughter BD, Huff JM, Wiegraebe W, et al. SAM domain-based protein oligomerization observed by live-cell fluorescence fluctuation spectroscopy. PLoS One. 2008;**3**:e1931

[79] Youker RT, Bruns JR, Costa SA, et al. Multiple motifs regulate apical sorting of p75 via a mechanism that involves dimerization and higher-order oligomerization. Molecular Biology of the Cell. 2013;**24**:1996-2007

[80] Malengo G, Andolfo A, Sidenius N, et al. Fluorescence correlation spectroscopy and photon counting histogram on membrane proteins: Functional dynamics of the glycosylphosphatidylinositol-anchored urokinase plasminogen activator receptor. Journal of Biomedical Optics. 2008;**13**:031215

[81] Herrick-Davis K, Grinde E, Lindsley T, et al. Oligomer size of the serotonin 5-Hydroxytryptamine 2C (5-HT_{2C}) receptor revealed by fluorescence correlation spectroscopy with photon counting histogram analysis: Evidence for homodimers without monomers or tetramers. Journal of Biological Chemistry. 2012;**287**:23604-23614

[82] Herrick-Davis K, Grinde E, Cowan A, et al. Fluorescence correlation spectroscopy analysis of serotonin, adrenergic, muscarinic, and dopamine receptor dimerization: The oligomer number puzzle. Molecular Pharmacology. 2013;**84**:630-642

[83] Herrick-Davis K, Grinde E, Lindsley T, et al. Native serotonin 5-HT2C receptors are expressed as homodimers on the apical surface of choroid plexus epithelial cells. Molecular Pharmacology. 2015;**87**:660-673

[84] Rudiger M, Haupts U, Moore KJ, et al. Single-molecule detection technologies in miniaturized high throughput screening: Binding assays for G protein-coupled receptors using fluorescence intensity distribution analysis and fluorescence anisotropy. Journal of Biomolecular Screening. 2001;**6**:29-37

[85] Sanchez-Andres A, Chen Y, Müller JD. Molecular brightness determined from a generalized form of Mandel's Q-parameter. Biophysical Journal. 2005;**89**:3531-3547

[86] Qian H, Elson EL. On the analysis of high order moments of fluorescence fluctuations. Biophysical Journal. 1990;**57**:375-380

[87] Mandel L. Sub-Poissonian photon statistics in resonance fluorescence. Optics Letters. 1979;**4**:205

[88] Hur K-H, Macdonald PJ, Berk S, et al. Quantitative measurement of brightness from living cells in the presence of photodepletion. PLoS One. 2014;**9**:e97440

[89] Hur K-H, Mueller JD. Quantitative brightness analysis of fluorescence intensity fluctuations in *E. coli*. Plos One. 2015;**10**:e0130063

[90] Müller JD. Cumulant analysis in fluorescence fluctuation spectroscopy. Biophysical Journal. 2004;**86**:3981-3992

[91] Perroud TD, Huang B, Zare RN. Effect of bin time on the photon counting histogram for one-photon excitation. ChemPhysChem. 2005;**6**:905-912

[92] Palo K, Mets Ü, Jäger S, et al. Fluorescence intensity multiple distributions analysis: Concurrent determination of diffusion times and molecular brightness. Biophysical Journal. 2000;**79**:2858-2866

[93] Wu B, Müller JD. Time-integrated fluorescence cumulant analysis in fluorescence fluctuation spectroscopy. Biophysical Journal. 2005;**89**:2721-2735

[94] Wu B, Singer RH, Mueller JD. Time-integrated fluorescence cumulant analysis and its application in living cells. In: Methods in Enzymology. Amsterdam, Netherlands: Elsevier; 2013;**518**:99-119

[95] Melnykov AV, Hall KB. Revival of high-order fluorescence correlation analysis: Generalized theory and biochemical applications. The

Journal of Physical Chemistry B. 2009;**113**:15629-15638

[96] Scales N, Swain PS. Resolving fluorescent species by their brightness and diffusion using correlated photon-counting histograms. PLoS One. 2019;**14**:e0226063

[97] Chen Y, Tekmen M, Hillesheim L, et al. Dual-color photon-counting histogram. Biophysical Journal. 2005;**88**:2177-2192

[98] Palo K, Brand L, Eggeling C, et al. Fluorescence intensity and lifetime distribution analysis: Toward higher accuracy in fluorescence fluctuation spectroscopy. Biophysical Journal. 2002;**83**:605-618

[99] Laurence TA, Kapanidis AN, Kong X, et al. Photon arrival-time interval distribution (PAID): A novel tool for analyzing molecular interactions. The Journal of Physical Chemistry B. 2004;**108**:3051-3067

[100] Koppel DE, Morgan F, Cowan AE, et al. Scanning concentration correlation spectroscopy using the confocal laser microscope. Biophysical Journal. 1994;**66**:502-507

[101] Ohsugi Y, Kinjo M. Multipoint fluorescence correlation spectroscopy with total internal reflection fluorescence microscope. Journal of Biomedical Optics. 2009;**14**:014030

[102] Singh AP, Krieger JW, Buchholz J, et al. The performance of 2D array detectors for light sheet based fluorescence correlation spectroscopy. Optics Express. 2013;**21**:8652

[103] Gösch M, Serov A, Anhut T, et al. Parallel single molecule detection with a fully integrated single-photon 2×2 CMOS detector array. Journal of Biomedical Optics. 2004;**9**:913

[104] Blom H, Johansson M, Hedman A-S, et al. Parallel fluorescence detection of single biomolecules in microarrays by a diffractive-optical-designed 2×2 fan-out element. Applied Optics. 2002;**41**:3336

[105] Colyer RA, Scalia G, Rech I, et al. High-throughput FCS using an LCOS spatial light modulator and an 8×1 SPAD array. Biomedical Optics Express. 2010;**1**:1408

[106] Burkhardt M, Schwille P. Electron multiplying CCD based detection for spatially resolved fluorescence correlation spectroscopy. Optics Express. 2006;**14**:5013

[107] Colyer RA, Scalia G, Villa FA, et al. Ultra high-throughput single molecule spectroscopy with a 1024 pixel SPAD. In: Enderlein J, Gryczynski ZK, Erdmann R, editors. Single Molecule Spectroscopy and Imaging IV. Vol. 7905. San Francisco, California, USA: SPIE Proceedings; 2011. p. 790503

[108] Kloster-Landsberg M, Herbomel G, Wang I, et al. Cellular response to heat shock studied by multiconfocal fluorescence correlation spectroscopy. Biophysical Journal. 2012;**103**:1110-1119

[109] Sisan DR, Arevalo R, Graves C, et al. Spatially resolved fluorescence correlation spectroscopy using a spinning disk confocal microscope. Biophysical Journal. 2006;**91**:4241-4252

[110] Wohland T, Shi X, Sankaran J, et al. Single plane illumination fluorescence correlation spectroscopy (SPIM-FCS) probes inhomogeneous three-dimensional environments. Optics Express. 2010;**18**:10627

[111] Buchholz J, Krieger J, Bruschini C, et al. Widefield high frame rate single-photon SPAD imagers for SPIM-FCS. Biophysical Journal. 2018;**114**:2455-2464

[112] Krieger JW, Singh AP, Garbe CS, et al. Dual-color fluorescence cross-correlation spectroscopy on a single plane illumination microscope (SPIM-FCCS). Optics Express. 2014;**22**:2358-2375

[113] Wachsmuth M, Conrad C, Bulkescher J, et al. High-throughput fluorescence correlation spectroscopy enables analysis of proteome dynamics in living cells. Nature Biotechnology. 2015;**33**:384-389

[114] Fu X, Song Y, Masud A, et al. High-throughput fluorescence correlation spectroscopy enables analysis of surface components of cell-derived vesicles. Analytical and Bioanalytical Chemistry. 2020;**412**:2589-2597

[115] Digman MA, Brown CM, Sengupta P, et al. Measuring fast dynamics in solutions and cells with a laser scanning microscope. Biophysical Journal. 2005;**89**:1317-1327

[116] Digman MA, Wiseman PW, Choi C, et al. Stoichiometry of molecular complexes at adhesions in living cells. Proceedings of the National Academy of Sciences. 2009;**106**:2170-2175

[117] Brown CM, Dalal RB, Hebert B, et al. Raster image correlation spectroscopy (RICS) for measuring fast protein dynamics and concentrations with a commercial laser scanning confocal microscope. Journal of Microscopy. 2008;**229**:78-91

[118] Suzuki T, Ainai A, Nagata N, et al. A novel function of the N-terminal domain of PA in assembly of influenza a virus RNA polymerase. Biochemical and Biophysical Research Communications. 2011;**414**:719-726

[119] Brejchová J, Sýkora J, Ostašov P, et al. TRH-receptor mobility and function in intact and cholesterol-depleted plasma membrane of HEK293 cells stably expressing TRH-R-eGFP. Biochimica et Biophysica Acta (BBA) - Biomembranes. 2015;**1848**:781-796

[120] Laňková M, Humpolíčková J, Vosolsobě S, et al. Determination of dynamics of plant plasma membrane proteins with fluorescence recovery and raster image correlation spectroscopy. Microscopy and Microanalysis. 2016;**22**:290-299

[121] Begarani F, D'Autilia F, Signore G, et al. Capturing metabolism-dependent solvent dynamics in the lumen of a trafficking lysosome. ACS Nano. 23 January 2019. DOI: 10.1021/acsnano.8b07682. [Epub ahead of print]

[122] Norris SCP, Humpolíčková J, Amler E, et al. Raster image correlation spectroscopy as a novel tool to study interactions of macromolecules with nanofiber scaffolds. Acta Biomaterialia. 2011;**7**:4195-4203

[123] Digman MA, Wiseman PW, Horwitz AR, et al. Detecting protein complexes in living cells from laser scanning confocal image sequences by the cross correlation raster image spectroscopy method. Biophysical Journal. 2009;**96**:707-716

[124] Digman MA, Gratton E. Scanning image correlation spectroscopy. BioEssays. 2012;**34**:377-385

[125] Sasaki A, Yamamoto J, Jin T, et al. Raster image cross-correlation analysis for spatiotemporal visualization of intracellular degradation activities against exogenous DNAs. Scientific Reports. November 2015;**5**:1-9. Article ID: 14428. DOI: 10.1038/srep14428. [Epub ahead of print]

[126] Hendrix J, Lamb DC. Implementation and application of pulsed interleaved excitation for dual-color FCS and RICS. Methods in Molecular Biology. 2014;**1076**:653-682

[127] Choi CK, Zareno J, Digman MA, et al. Cross-correlated fluctuation

analysis reveals phosphorylation-regulated paxillin-FAK complexes in nascent adhesions. Biophysical Journal. 2011;**100**:583-592

[128] Kapoor-Kaushik N, Hinde E, Compeer EB, et al. Distinct mechanisms regulate Lck spatial organization in activated T cells. Frontiers in Immunology. 2016;**7**:83

[129] Dobrinskikh E, Lanzano L, Rachelson J, et al. Shank2 contributes to the apical retention and intracellular redistribution of NaPiIIa in OK cells. American Journal of Physiology: Cell Physiology. 2013;**304**:C561-C573

[130] Schrimpf W, Lemmens V, Smisdom N, et al. Crosstalk-free multicolor RICS using spectral weighting. Methods. 2018;**140-141**:97-111

[131] Longfils M, Smisdom N, Ameloot M, et al. Raster image correlation spectroscopy performance evaluation. Biophysical Journal. 2019;**117**:1900-1914

[132] Kolin DL, Wiseman PW. Advances in image correlation spectroscopy: Measuring number densities, aggregation states, and dynamics of fluorescently labeled macromolecules in cells. Cell Biochemistry and Biophysics. 2007;**49**:141-164

[133] Wiseman PW. Image correlation spectroscopy: Principles and applications. Cold Spring Harbor Protocols. 2015;**2015**:336-348

[134] Petersen NO, Höddelius PL, Wiseman PW, et al. Quantitation of membrane receptor distributions by image correlation spectroscopy: Concept and application. Biophysical Journal. 1993;**65**:1135-1146

[135] Keating E, Nohe A, Petersen NO. Studies of distribution, location and dynamic properties of EGFR on the cell surface measured by image correlation spectroscopy. European Biophysics Journal. 2008;**37**:469-481

[136] Srivastava M, Petersen NO. Diffusion of transferrin receptor clusters. Biophysical Chemistry. 1998;**75**:201-211

[137] Hebert B, Costantino S, Wiseman PW. Spatiotemporal image correlation spectroscopy (STICS) theory, verification, and application to protein velocity mapping in living CHO cells. Biophysical Journal. 2005;**88**:3601-3614

[138] Wiseman PW. Spatial mapping of integrin interactions and dynamics during cell migration by image correlation microscopy. Journal of Cell Science. 2004;**117**:5521-5534

[139] Toplak T, Pandzic E, Chen L, et al. STICCS reveals matrix-dependent adhesion slipping and gripping in migrating cells. Biophysical Journal. 2012;**103**:1672-1682

[140] Kolin DL, Costantino S, Wiseman PW. Sampling effects, noise, and photobleaching in temporal image correlation spectroscopy. Biophysical Journal. 2006;**90**:628-639

[141] Kolin DL, Ronis D, Wiseman PW. k-space image correlation spectroscopy: A method for accurate transport measurements independent of fluorophore photophysics. Biophysical Journal. 2006;**91**:3061-3075

[142] Abu-Arish A, Pandžić E, Kim D, et al. Agonists that stimulate secretion promote the recruitment of CFTR into membrane lipid microdomains. Journal of General Physiology. 2019;**151**:834-849

[143] Digman MA, Dalal R, Horwitz AF, et al. Mapping the number of molecules and brightness in the laser scanning microscope. Biophysical Journal. 2008;**94**:2320-2332

[144] Unruh JR, Gratton E. Analysis of molecular concentration and brightness from fluorescence fluctuation data with an electron multiplied CCD camera. Biophysical Journal. 2008;**95**:5385-5398

[145] Macdonald P, Johnson J, Smith E, et al. Brightness analysis. In: Methods in Enzymology. Vol. 518. Academic Press (imprint of Elsevier). pp. 71-98

[146] Adu-Gyamfi E, Digman MA, Gratton E, et al. Investigation of Ebola VP40 assembly and oligomerization in live cells using number and brightness analysis. Biophysical Journal. 2012;**102**:2517-2525

[147] James NG, Digman MA, Gratton E, et al. Number and brightness analysis of LRRK2 oligomerization in live cells. Biophysical Journal. 2012;**102**:L41-L43

[148] Ossato G, Digman MA, Aiken C, et al. A two-step path to inclusion formation of Huntingtin peptides revealed by number and brightness analysis. Biophysical Journal. 2010;**98**:3078-3085

[149] Mieruszynski S, Briggs C, Digman MA, et al. Live cell characterization of DNA aggregation delivered through lipofection. Scientific Reports. September 2015;**5**:1-9. Article ID: 10528. DOI: 10.1038/srep10528. [Epub ahead of print]

[150] Sameni S, Zhang R, Digman MA. Number and molecular brightness analysis reveals Htt25Q protein aggregation upon the uptake of Htt97Q aggregates. Biochemical and Biophysical Research Communications. 2020;**522**:133-137

[151] Adu-Gyamfi E, Soni S, Jee C, et al. A loop region in the N-terminal domain of Ebola virus VP40 is important in viral assembly, budding, and egress. Viruses. 2014;**6**:3837-3854

[152] Bachir AI, Zareno J, Moissoglu K, et al. Integrin-associated complexes form hierarchically with variable stoichiometry in nascent adhesions. Current Biology. 2014;**24**:1845-1853

[153] Lagarrigue F, Vikas Anekal P, Lee H-S, et al. A RIAM/lamellipodin–talin–integrin complex forms the tip of sticky fingers that guide cell migration. Nature Communications. December 2015;**6**:8492. DOI: 10.1038/ncomms9492. [Epub ahead of print]

[154] Hortigüela V, Larrañaga E, Cutrale F, et al. Nanopatterns of surface-bound EphrinB1 produce multivalent ligand–receptor interactions that tune EphB2 receptor clustering. Nano Letters. 2018;**18**:629-637

[155] Cutrale F, Rodriguez D, Hortigüela V, et al. Using enhanced number and brightness to measure protein oligomerization dynamics in live cells. Nature Protocols. 2019;**14**:616-638

[156] Barbeau A, Swift JL, Godin AG, et al. Spatial intensity distribution analysis (SpIDA). In: Methods in Cell Biology. Amsterdam, Netherlands: Elsevier. 2013;**117**:1-19

[157] Godin AG, Costantino S, Lorenzo L-E, et al. Revealing protein oligomerization and densities in situ using spatial intensity distribution analysis. Proceedings of the National Academy of Sciences. 2011;**108**:7010-7015

[158] Godin AG, Rappaz B, Potvin-Trottier L, et al. Spatial intensity distribution analysis reveals abnormal oligomerization of proteins in single cells. Biophysical Journal. 2015;**109**:710-721

[159] Hamrang Z, McGlynn HJ, Clarke D, et al. Monitoring the kinetics of CellTrace™ calcein red-orange AM intracellular accumulation with spatial intensity distribution analysis.

Biochimica et Biophysica Acta (BBA) - General Subjects. 2014;**1840**:2914-2923

[160] Ward RJ, Pediani JD, Harikumar KG, et al. Spatial intensity distribution analysis quantifies the extent and regulation of homodimerization of the secretin receptor. The Biochemical Journal. 2017;**474**:1879-1895

[161] Rattray Z, Zindy E, Buzza KM, et al. Evaluation of temporal aggregation processes using spatial intensity distribution analysis. In: McManus JJ, editor. Protein Self-Assembly. New York, NY: Springer New York. 2019. pp. 141-155

[162] Stoneman MR, Biener G, Ward RJ, et al. A general method to quantify ligand-driven oligomerization from fluorescence-based images. Nature Methods. 2019;**16**:493-496

[163] Stoneman MR, Biener G, Raicu V. Reply to: Spatial Heterogeneity Molecular brightness. Biophysics. 11 November 2019. DOI: 10.1101/822296. Preprint. [Epub ahead of print]

[164] Hennen J, Hur K-H, Saunders CA, et al. Quantitative brightness analysis of protein oligomerization in the nuclear envelope. Biophysical Journal. 2017;**113**:138-147

[165] Stasevich TJ, Mueller F, Michelman-Ribeiro A, et al. Cross-validating FRAP and FCS to quantify the impact of photobleaching on in vivo binding estimates. Biophysical Journal. 2010;**99**:3093-3101

[166] Ries J, Schwille P. New concepts for fluorescence correlation spectroscopy on membranes. Physical Chemistry Chemical Physics. 2008;**10**:3487

[167] Ries J, Bayer M, Csúcs G, et al. Automated suppression of sample-related artifacts in fluorescence correlation spectroscopy. Optics Express. 2010;**18**:11073

[168] Kilpatrick LE, Briddon SJ, Holliday ND. Fluorescence correlation spectroscopy, combined with bimolecular fluorescence complementation, reveals the effects of β-arrestin complexes and endocytic targeting on the membrane mobility of neuropeptide Y receptors. Biochimica et Biophysica Acta (BBA) - Molecular Cell Research. 2012;**1823**:1068-1081

[169] Khmelinskaia A, Mücksch J, Conci F, et al. FCS analysis of protein mobility on lipid monolayers. Biophysical Journal. 2018;**114**:2444-2454

[170] Ozgen H, Schrimpf W, Hendrix J, et al. The lateral membrane organization and dynamics of myelin proteins PLP and MBP are dictated by distinct galactolipids and the extracellular matrix. PLoS One. 2014;**9**:e101834

[171] Nolan R, Iliopoulou M, Alvarez L, et al. Detecting protein aggregation and interaction in live cells: A guide to number and brightness. Methods. 2018;**140-141**:172-177

[172] Bakker E, Swain PS. Estimating numbers of intracellular molecules through analysing fluctuations in photobleaching. Scientific Reports. December 2019;**9**. DOI: 10.1038/s41598-019-50921-7. [Epub ahead of print]

[173] Trullo A, Corti V, Arza E, et al. Application limits and data correction in number of molecules and brightness analysis: N&B-limits and corrections. Microscopy Research and Technique. 2013;**76**:1135-1146

[174] Lange JJ, Wood CJ, Marshall WA, et al. Correction of bleaching artifacts in high content fluorescence correlation spectroscopy (HCS-FCS) data. In: Enderlein J, Gregor I, Gryczynski ZK, et al., editors. Single Molecule Spectroscopy and Superresolution Imaging VI. San Francisco, California, USA: SPIE Proceedings; 2013. p. 859006

[175] Nolan R, Iliopoulou M, Siebold C, et al. Robin Hood: Non-fitting, non-smoothing image detrending for bleaching correction. bioRxiv. 14 June 2019:1-13. DOI: 10.1101/667824. Preprint, [Epub ahead of print]

[176] Ishii K, Tahara T. Correction of the afterpulsing effect in fluorescence correlation spectroscopy using time symmetry analysis. Optics Express. 2015;**23**:32387

[177] Hillesheim LN, Müller JD. The dual-color photon counting histogram with non-ideal photodetectors. Biophysical Journal. 2005;**89**:3491-3507

[178] Ziarkash AW, Joshi SK, Stipčević M, et al. Comparative study of afterpulsing behavior and models in single photon counting avalanche photo diode detectors. Scientific Reports. December 2018;**8**(5076):1-8. DOI: 10.1038/s41598-018-23398-z. [Epub ahead of print]

[179] Fukushima R, Yamamoto J, Ishikawa H, et al. Two-detector number and brightness analysis reveals spatio-temporal oligomerization of proteins in living cells. Methods. 2018;**140-141**:161-171

[180] Foo YH, Naredi-Rainer N, Lamb DC, et al. Factors affecting the quantification of biomolecular interactions by fluorescence cross-correlation spectroscopy. Biophysical Journal. 2012;**102**:1174-1183

[181] Widengren J, Mets U, Rigler R. Fluorescence correlation spectroscopy of triplet states in solution: A theoretical and experimental study. The Journal of Physical Chemistry. 1995;**99**:13368-13379

[182] Balleza E, Kim JM, Cluzel P. Systematic characterization of maturation time of fluorescent proteins in living cells. Nature Methods. 2018;**15**:47-51

[183] Dunsing V, Luckner M, Zühlke B, et al. Optimal fluorescent protein tags for quantifying protein oligomerization in living cells. Scientific Reports. December 2018;**8**. DOI: 10.1038/s41598-018-28858-0. [Epub ahead of print]

[184] Hendrix J, Flors C, Dedecker P, et al. Dark states in monomeric red fluorescent proteins studied by fluorescence correlation and single molecule spectroscopy. Biophysical Journal. 2008;**94**:4103-4113

[185] Hern JA, Baig AH, Mashanov GI, et al. Formation and dissociation of M1 muscarinic receptor dimers seen by total internal reflection fluorescence imaging of single molecules. Proceedings of the National Academy of Sciences. 2010;**107**:2693-2698

[186] Chun L, Zhang W, Liu J. Structure and ligand recognition of class C GPCRs. Acta Pharmacologica Sinica. 2012;**33**:312-323

[187] Ferré S, Casadó V, Devi LA, et al. G protein–coupled receptor oligomerization revisited: Functional and pharmacological perspectives. Pharmacological Reviews. 2014;**66**:413-434

[188] Milligan G, Ward RJ, Marsango S. GPCR homo-oligomerization. Current Opinion in Cell Biology. 2019;**57**:40-47

[189] Nenasheva TA, Neary M, Mashanov GI, et al. Abundance, distribution, mobility and oligomeric state of M2 muscarinic acetylcholine receptors in live cardiac muscle. Journal of Molecular and Cellular Cardiology. 2013;**57**:129-136

[190] Redka DS, Morizumi T, Elmslie G, et al. Coupling of G proteins to reconstituted monomers and tetramers of the M_2 muscarinic receptor. Journal of Biological Chemistry. 2014;**289**:24347-24365

[191] Shivnaraine RV, Kelly B, Sankar KS, et al. Allosteric modulation in monomers and oligomers of a G protein-coupled receptor. eLife. 6 May 2016;**5**:1-26, e11685. DOI: 10.7554/eLife.11685. [Epub ahead of print]

[192] Walsh SM, Mathiasen S, Christensen SM, et al. Single proteoliposome high-content analysis reveals differences in the homo-oligomerization of GPCRs. Biophysical Journal. 2018;**115**:300-312

[193] Marsango S, Caltabiano G, Jiménez-Rosés M, et al. A molecular basis for selective antagonist destabilization of dopamine D3 receptor quaternary organization. Scientific Reports. May 2017;7:1-17, 2134. DOI: 10.1038/s41598-017-02249-3. [Epub ahead of print]

[194] Ward RJ, Pediani JD, Godin AG, et al. Regulation of oligomeric organization of the serotonin 5-hydroxytryptamine 2C (5-HT_{2C}) receptor observed by spatial intensity distribution analysis. Journal of Biological Chemistry. 2015;**290**:12844-12857

[195] Shivnaraine RV, Fernandes DD, Ji H, et al. Single-molecule analysis of the supramolecular organization of the M_2 muscarinic receptor and the $G\alpha_{i1}$ protein. Journal of the American Chemical Society. 2016;**138**:11583-11598

[196] Pathak A, Smih F, Galinier M, et al. Insulin downregulates M2-muscarinic receptors in adult rat atrial cardiomyocytes: A link between obesity and cardiovascular complications. International Journal of Obesity. 2005;**29**:176-182

[197] Pediani JD, Ward RJ, Godin AG, et al. Dynamic regulation of quaternary organization of the M_1 muscarinic receptor by subtype-selective antagonist drugs. Journal of Biological Chemistry. 2016;**291**:13132-13146

[198] Head BP, Patel HH, Roth DM, et al. Microtubules and actin microfilaments regulate lipid raft/caveolae localization of adenylyl cyclase signaling components. Journal of Biological Chemistry. 2006;**281**:26391-26399

[199] Patowary S, Alvarez-Curto E, Xu T-R, et al. The muscarinic M3 acetylcholine receptor exists as two differently sized complexes at the plasma membrane. Biochemical Journal. 2013;**452**:303-312

[200] Armbruster BN, Li X, Pausch MH, et al. Evolving the lock to fit the key to create a family of G protein-coupled receptors potently activated by an inert ligand. Proceedings of the National Academy of Sciences. 2007;**104**:5163-5168

[201] Snapp EL. When is a monomer not a monomer? The top three ways your favorite fluorescent protein oligomerizes in cells. 2016. Available from: https://blog.addgene.org/when-is-a-monomer-not-a-monomer-the-top-three-ways-your-favorite-fluorescent-protein-oligomerizes-in-cells [Accessed: 04 June 2020]

[202] Mueller A, Mahmoud NG, Goedecke MC, et al. Pharmacological characterization of the chemokine receptor, CCR5. British Journal of Pharmacology. 2002;**135**:1033-1043

[203] Harikumar KG, Pinon DI, Miller LJ. Transmembrane segment IV contributes a functionally important interface for oligomerization of the class II G protein-coupled secretin receptor. Journal of Biological Chemistry. 2007;**282**:30363-30372

[204] Golebiewska U, Johnston JM, Devi L, et al. Differential response to morphine of the oligomeric state of μ-opioid in the presence of δ-opioid receptors. Biochemistry. 2011;**50**:2829-2837

[205] Briddon SJ, Gandía J, Amaral OB, et al. Plasma membrane diffusion of g protein-coupled receptor oligomers. Biochimica et Biophysica Acta (BBA) - Molecular Cell Research. 2008;**1783**:2262-2268

[206] Briddon SJ, Middleton RJ, Cordeaux Y, et al. Quantitative analysis of the formation and diffusion of A1-adenosine receptor-antagonist complexes in single living cells. Proceedings of the National Academy of Sciences. 2004;**101**:4673-4678

[207] Philip F, Sengupta P, Scarlata S. Signaling through a G protein-coupled receptor and its corresponding G protein follows a stoichiometrically limited model. Journal of Biological Chemistry. 2007;**282**:19203-19216

[208] Licht SS, Sonnleitner A, Weiss S, et al. A rugged energy landscape mechanism for trapping of transmembrane receptors during endocytosis †. Biochemistry. 2003;**42**:2916-2925

[209] Kaiser SM, Quinn RJ. Adenosine receptors as potential therapeutic targets. Drug Discovery Today. 1999;**4**:542-551

[210] Briddon SJ, Middleton RJ, Yates AS, et al. Application of fluorescence correlation spectroscopy to the measurement of agonist binding to a G-protein coupled receptor at the single cell level. Faraday Discussions. 2004;**126**:197

[211] Marceau F, Bachelard H, Bouthillier J, et al. Bradykinin receptors: Agonists, antagonists, expression, signaling, and adaptation to sustained stimulation. International Immunopharmacology. 2020;**82**:106305

[212] Brothers SP, Wahlestedt C. Therapeutic potential of neuropeptide Y (NPY) receptor ligands. EMBO Molecular Medicine. 2010;**2**(11):429-439

[213] Zacharias DA. Partitioning of lipid-modified monomeric GFPs into membrane microdomains of live cells. Science. 2002;**296**:913-916

[214] Zakrys L, Ward RJ, Pediani JD, et al. Roundabout 1 exists predominantly as a basal dimeric complex and this is unaffected by binding of the ligand Slit2. Biochemical Journal. 2014;**461**:61-73

[215] Grove J, Metcalf DJ, Knight AE, et al. Flat clathrin lattices: Stable features of the plasma membrane. Molecular Biology of the Cell. 2014;**25**:3581-3594

[216] Pontes B, Monzo P, Gauthier NC. Membrane tension: A challenging but universal physical parameter in cell biology. Seminars in Cell & Developmental Biology. 2017;**71**:30-41

[217] Mondal S, Johnston JM, Wang H, et al. Membrane driven spatial organization of GPCRs. Scientific Reports. December 2013;**3**. DOI: 10.1038/srep02909. [Epub ahead of print]

[218] Botelho AV, Huber T, Sakmar TP, et al. Curvature and hydrophobic forces drive oligomerization and modulate activity of rhodopsin in membranes. Biophysical Journal. 2006;**91**:4464-4477

[219] Dai J, Sheetz MP. Membrane tether formation from blebbing cells. Biophysical Journal. 1999;**77**:3363-3370

[220] Boulant S, Kural C, Zeeh J-C, et al. Actin dynamics counteract membrane tension during clathrin-mediated endocytosis. Nature Cell Biology. 2011;**13**:1124-1131

[221] Annibale P, Lohse MJ. Spatial heterogeneity in molecular brightness. Nature Methods. 2020;**17**:273-275

[222] Annibale P, Lohse MJ. Molecular Brightness analysis of GPCR oligomerization in the presence of spatial heterogeneity. 2019. arXiv:190710841 [physics, q-bio]. Available from: http://arxiv.org/abs/1907.10841. [Accessed: 05 June 2020]

[223] Sadegh S, Higgins JL, Mannion PC, et al. Plasma membrane is compartmentalized by a self-similar cortical actin meshwork. Physical Review X. 9 March 2017;7:1-10, 011031. DOI: 10.1103/PhysRevX.7.011031. [Epub ahead of print]